

1 **High-throughput profiling of drug interactions in Gram-positive bacteria**

2 Elisabetta Cacace¹, Vladislav Kim^{1,2}, Michael Knopp¹, Manuela Tietgen³, Amber Brauer-
3 Nikonow¹, Kemal Inecik¹, André Mateus¹, Alessio Milanese^{4,5}, Marita Torrisen Mårlid⁶, Karin
4 Mitosch¹, Joel Selkirk^{1,8}, Ana Rita Brochado^{1,9}, Oscar P. Kuipers⁷, Morten Kjos⁶, Georg Zeller⁴,
5 Mikhail M. Savitski¹, Stephan Göttig³, Wolfgang Huber¹, Athanasios Typas^{1,4*}

6

7 ¹Genome Biology Unit, European Molecular Biology Laboratory, Heidelberg, Germany.

8 ²Collaboration for joint PhD degree between EMBL and Heidelberg University, Faculty of
9 Biosciences, Heidelberg, Germany.

10 ³Institute of Medical Microbiology and Infection Control, Hospital of Goethe University,
11 Frankfurt am Main, Germany.

12 ⁴Structural and Computational Biology Unit, European Molecular Biology Laboratory,
13 Heidelberg, Germany.

14 ⁵Institute of Microbiology and Swiss Institute of Bioinformatics, Department of Biology, ETH-
15 Zürich, Zürich, Switzerland.

16 ⁶Faculty of Chemistry, Biotechnology and Food Science, Norwegian University of Life
17 Sciences, Ås, Norway.

18 ⁷Department of Molecular Genetics, Groningen Molecular Biology and Biotechnology Institute,
19 University of Groningen, Groningen, The Netherlands.

20 ⁸Current address: Institute for Medical Microbiology, RWTH University Hospital, Aachen,
21 Germany.

22 ⁹Current address: Microbiology, Biocenter, University of Würzburg, Würzburg, Germany.

23

24 *Correspondence: typas@embl.de

25 **Abstract**

26 Drug combinations present a powerful strategy to tackle antimicrobial resistance, but have not
27 been systematically tested in many bacterial species. Here, we used an automated high-
28 throughput setup to profile ~ 8000 combinations between 65 antibacterial drugs in three Gram-
29 positive species: the model species, *Bacillus subtilis* and two prominent pathogens,
30 *Staphylococcus aureus* and *Streptococcus pneumoniae*. Thereby, we recapitulate previously
31 known drug interactions, but also identify ten times more interactions than previously reported
32 in the pathogen *S. aureus*, including two synergies that were also effective in multi-drug
33 resistant clinical *S. aureus* isolates *in vitro* and *in vivo*. Interactions were largely species-
34 specific and mostly synergistic for drugs targeting the same cellular process, as observed also
35 for Gram-negative species¹. Yet, the dominating synergies are clearly distinct between Gram-
36 negative and Gram-positive species, and are driven by different bottlenecks in drug uptake
37 and vulnerabilities of their cell surface structures. To further explore interactions of commonly
38 prescribed non-antibiotic drugs with antibiotics, we tested 2728 of such combinations in *S.*
39 *aureus*, detecting a plethora of unexpected antagonisms that could compromise the efficacy
40 of antimicrobial treatments in the age of polypharmacy. We uncovered even more synergies
41 than antagonisms, some of which we could demonstrate as effective combinations *in vivo*
42 against multi-drug resistant clinical isolates. Among them, we showed that the antiaggregant
43 ticagrelor interferes with purine metabolism and changes the surface charge of *S. aureus*,
44 leading to strong synergies with cationic antibiotics. Overall, this exemplifies the untapped
45 potential of approved non-antibacterial drugs to be repurposed as antibiotic adjuvants. All data
46 can be browsed through an interactive interface (<https://apps.embl.de/combact/>).

47 **Introduction**

48 Antibacterial agents have been used in combination since the dawn of the antibiotic era for
49 different purposes: to achieve synergy (e.g. sulfamethoxazole-trimethoprim), to limit
50 resistance (e.g. combinations of beta-lactams and beta-lactamase inhibitors, or antitubercular
51 regimens), and/or to broaden the spectrum of action of anti-infective treatments (e.g. empiric
52 treatments of sepsis)². With antimicrobial resistance (AMR) posing a global threat to public
53 health, which permeates all domains of modern medicine^{3,4}, the use of drug combinations to
54 re-sensitize resistant strains has emerged as one of the promising means to bypass the
55 stagnant drug discovery pipeline⁵.

56

57 Although a few antibacterial combinations are used in clinics, and screens for approved
58 compounds as adjuvants for antibiotics have been increasingly conducted in the last decade^{6–}
59 ¹¹, the full potential of drug combinations for treating bacterial pathogens remains
60 underexplored. This is because the combinatorial space is vast, and drug interactions are rare,
61 and concentration-, drug-, time-, species- and even strain-specific^{1,12,13}, making systematic
62 testing necessary, yet highly demanding. As a result, drug interactions have not yet been
63 systematically profiled in many clinically relevant bacterial species.

64

65 With the increase of polypharmacy¹⁴, antibiotics are often prescribed in combination with other
66 drugs¹⁵. While pharmacokinetic interactions between antibiotics and non-antibiotic drugs are
67 well-known for the host (e.g. dependencies on drug metabolism and excretion by the liver and
68 the kidney)¹⁶, they are poorly characterized at the level of bacterial physiology.

69

70 We recently used automated platforms to systematically profile antibiotic interactions on three
71 Gram-negative pathogens¹. Here, we expanded this experimental and computational
72 framework to generate a comprehensive resource of drug interactions in three Gram-positive
73 bacterial species: the pathogens *Staphylococcus aureus* and *Streptococcus pneumoniae*, two

74 of the most prominent antibiotic-resistant bacteria^{3,17}, and the model organism *Bacillus subtilis*.
75 Compared to previous interaction studies in Gram-positive species^{8,10,18}, this vastly increased
76 the number of drugs, concentrations and strains tested. By probing all main classes of
77 antibiotics, we could relate interaction outcomes to bacterial structural features, cellular
78 network architecture, as well as to drug target conservation. Moreover, we profiled the
79 interactions of antibiotics with a large panel of non-antibiotic drugs in *S. aureus* to investigate
80 the impact of commonly administered medications on antibiotic efficacy. Thereby, we
81 uncovered both strong synergies that remained effective against multidrug-resistant clinical *S.*
82 *aureus* isolates, and widespread antagonisms that could compromise the efficacy of antibiotic
83 treatments.

84

85 **Results**

86 **An automated pipeline for high-throughput testing of drug combinations**

87 We profiled 1891-2070 drug combinations in a 4 x 4 dose matrix (two-fold dilution gradient) in
88 *Staphylococcus aureus*, *Streptococcus pneumoniae* and *Bacillus subtilis*. For *S. aureus*, two
89 strains (*S. aureus* Newman and DSM 20231) were probed to assess within-species
90 conservation (**Fig. 1a, Supplementary Table 1**). The drug panel (n = 65) included antibiotics
91 (n = 57) used against infections with Gram-positive bacteria and belonging to all main classes
92 and targeting different bacterial processes, and eight other bioactive molecules, such as
93 antifungals, drugs with human targets and food additives – depicted as non-antibiotics (**Fig.**
94 **1a, Supplementary Table 1**).

95

96 We measured growth in a broth microdilution format in microtiter plates using optical density
97 (OD_{595nm}) as a readout. Media and shaking conditions were different for each species
98 (Methods). Drug concentrations were tailored after measuring minimal inhibitory
99 concentrations (MICs) for each drug in the four strains, with the highest concentration
100 corresponding to the MIC in most cases, and the intermediate and lowest concentration

101 corresponding to half and a quarter of the highest concentration, respectively (Methods,
102 **Supplementary Table 1**). We derived fitness values in the presence of single drugs and drug
103 combinations, dividing single-time point OD_{595nm} values upon drug treatment by the
104 corresponding values of no-drug controls at the same time point. This time point was selected
105 according to the growth characteristics of each strain and aimed to capture both growth rate
106 and yield effects (Methods, **Extended Data Fig. 1**). We conducted all experiments in biological
107 (i.e. different overnight cultures) and technical (i.e. replicated wells in the same plate)
108 duplicates, achieving high replicate correlations (average Pearson correlation 0.84-0.89 for
109 biological (**Extended Data Fig. 2a-b**) and 0.91 for technical replicates (**Extended Data Fig.**
110 **2c**). Single time-point OD- and area under the growth-curve (AUC)-based fitness values led
111 to very similar results, with the former being more robust (**Extended Data Figs. 2d-e**).
112 Similarly, estimated single-drug fitness values mirrored experimentally-measured values and
113 were further used since they were derived from more measurements (**Extended Data Fig. 2f-**
114 **g**, Methods). From the 4 x 4 concentration matrices of fitness values, we calculated interaction
115 scores using the Bliss interaction model¹⁹ (Methods, **Extended Data Fig. 1**). For each pairwise
116 combination, a single effect size value was derived from the distribution of interaction scores,
117 consisting of at least 72 interaction scores including all replicates of individual concentration
118 combinations for each drug pair. The first and third quartile values of this distribution were
119 taken as effect size values for synergies and antagonisms, respectively, with negative values
120 corresponding to synergies and positive values to antagonisms (Methods, **Extended Data**
121 **Fig. 1, Supplementary Table 2**)¹. All the data is available for browsing in a user-friendly
122 interface (<https://apps.embl.de/combact/>).

123

124 To calibrate hit scoring, as well as to assess the high-throughput screen data quality, we
125 benchmarked the screen data against a validation set of 161 combinations (2% of screened
126 combinations), equally representing the four strains probed. These combinations were tested
127 in the same growth conditions as our high-throughput screen, but over a highly-resolved dose
128 space (8 x 8 matrix) of equally-spaced concentration dilution gradients (Methods, **Extended**

129 **Data Fig. 3a-b, Supplementary Table 2).** The precision-recall curves were comparable to the
130 previous Gram-negative screen¹, with highest precision (0.87) and recall (0.68) observed for
131 a threshold on absolute effect size of > 0.1 and on Benjamini-Hochberg adjusted p-value of <
132 0.05 (resampling procedure with 10,000 repetitions for each combination tested, comparison
133 with resampled Bliss scores using Wilcoxon rank-sum test in each iteration) (Methods,
134 **Extended Data Fig. 3c).** We were able to slightly increase the recall (0.72) by relaxing the
135 effect size thresholds for interactions found in both *S. aureus* strains, using within-species
136 conservation as an additional parameter to confirm interactions¹ (Methods, **Extended Data**
137 **Fig. 3c-d, Supplementary Table 2).**

138

139 **Drug interactions are rare and species-specific**

140 Antagonisms and synergies were detected to be equally prevalent across the three species,
141 accounting for ~12% of all combinations tested (**Fig. 1b**). This interaction rate, corrected by
142 our ability to observe synergies or antagonisms according to the fitness space probed for each
143 combination (Methods), is lower and less skewed towards antagonisms as compared to Gram-
144 negative species (*E. coli*, *S. Typhimurium*, *P. aeruginosa*)¹. This could be due to technical
145 (drug or strain selection biases) or biological (Gram-positive bacteria have a lower drug
146 permeability bottleneck than Gram-negative bacteria and hence less interactions will be
147 dependent on depend on intracellular drug availability¹) reasons.

148

149 Species-specificity of drug interactions has long been assumed²⁰, and recently systematically
150 demonstrated for Gram-negative species, with 30% of detected interactions shared between
151 at least two of the three species tested, and 5% conserved in all three species (*E. coli*, *S.*
152 *Typhimurium*, *P. aeruginosa*)¹. In Gram-positive species we observed an even lower
153 conservation rate (**Fig. 1c**), with only 81 out of 725 unique interactions (11.2%) conserved in
154 at least two species (**Fig. 1d**). 29 interactions were conserved in all three species (4%)
155 (**Supplementary Table 2**). We reasoned that the lower interspecies conservation in our
156 screen could be driven by the strain and species selection in the two screens, as for Gram-

157 negative species two closely-related enterobacteria, *E. coli* and *S. Typhimurium*, exhibited the
158 highest overlap of interactions¹. However, the interaction conservation rate of either of these
159 two species with *P. aeruginosa* is similar to the cross-species conservation rates we detected
160 for Gram-positive bacteria. Indeed, when we compared the interaction conservation rate and
161 genome sequence percentage identity (based on 40 universal single-copy marker genes²¹),
162 the two were significantly correlated (Methods, **Fig.1e**).

163

164 Synergies were shown to be more conserved in Gram-negative bacteria¹, but this trend was
165 non-significant in Gram-positive species, even after removing non-antibiotic drugs for which
166 intracellular targets and their conservation are unknown (**Extended Data Fig. 4a**). Conserved
167 synergies with Gram-positive species were mostly driven by drugs targeting the same
168 essential and highly conserved cellular processes, such as DNA biosynthesis and translation
169 (**Fig. 1d, Extended Data Fig. 4b**). Some of these interactions, such as the synergy between
170 macrolides and tetracyclines or between quinolones of different generations, have been
171 observed before in Gram-negative species^{1,22}, pointing towards conserved relationships
172 between the targets of these compounds. Similarly, the broad antagonism between drugs
173 targeting DNA and protein synthesis (**Fig. 1d**) is conserved in Gram-negative bacteria, and is
174 due to the alleviation of protein-DNA imbalance after treatment with any of the two antibiotics
175 alone²³. Overall, we detected 52 synergies and 66 antagonisms shared across the Gram-
176 positive/-negative divide (**Extended Data Fig. 4c-e, Supplementary Table 3**).

177

178 Numerous previously unknown drug synergies for *S. aureus*

179 We built separate interaction networks for each of the three species tested, and grouped drugs
180 according to their class or cellular target (**Fig. 2a-b; Extended Data Fig. 5**). Although
181 individual drug-drug interactions were only rarely conserved (**Fig. 1c**), interactions between
182 drug classes or targeted processes were more coherent in all three species. This functional
183 concordance became even clearer when comparing drugs based on all their interactions with
184 other drugs. Interaction-based clustering better recapitulated drug functional classes

185 (**Extended Data Fig. 6a**, Methods) than clustering based on chemical structures (**Extended**
186 **Data Fig. 6b**, Methods), suggesting that drug interactions capture more information on drug
187 mode of action than their chemical features.

188

189 Since *S. aureus* is the most relevant Gram-positive species in respect of AMR-attributable
190 deaths³, we systematically screened literature for reported drug interactions in this species.
191 Out of 331 unique interactions detected across the two *S. aureus* strains in our study, we
192 found only 31 to have been previously reported (**Fig. 2c**). 55 further interactions have been
193 reported in other bacterial species (**Supplementary Table 4**). Even when excluding those,
194 our dataset revealed 127 novel synergies for *S. aureus* (and 118 antagonisms), a third of
195 which (n = 39) was conserved in both strains. This confirms that the combinatorial space is a
196 largely unexplored reservoir for improving antimicrobial efficacy.

197

198 Known interactions include many conserved synergies between drugs with the same targets
199 (**Fig. 1d**), such as synergies between DNA-biosynthesis inhibitors, protein-synthesis
200 inhibitors, and cell-wall targeting antibiotics (**Fig. 2a-b**). Among these latter, we confirmed the
201 known synergy between cefepime and teicoplanin^{24,25}, and we validated it against several
202 MRSA (Methicillin-Resistant *S. aureus*) clinical isolates, including a strain resistant to the last-
203 resort antibiotic tigecycline (**Fig. 2d, Extended Data Fig. 7a**). When we infected larvae of the
204 greater wax moth *Galleria mellonella* with this MRSA strain, the combination protected the
205 animals from succumbing to the infection in contrast to single drug treatments (**Fig. 2e**),
206 confirming that the synergies are also effective *in vivo*.

207

208 Synergies between cell-wall targeting drugs and translation inhibitors are cornerstones of anti-
209 infective therapy against Gram-positive bacteria²⁶⁻²⁹. We could recapitulate some of these
210 synergies, but not the traditionally used combinations of beta-lactams and aminoglycosides.
211 This is in line with previously reported concerns on the general effectiveness of such type of
212 combinations, whose interaction outcome seems to be strikingly strain-specific³⁰⁻³³. Other cell-

213 wall targeting drugs may hold some unexplored potential: for instance, fosfomycin strongly
214 synergized with a diverse range of protein-synthesis inhibitors (**Supplementary Table 4**), and
215 could present an underexploited therapeutic resource against *S. aureus* (see Discussion).

216

217 Among the 300 previously unknown interactions we detected, 19 out of 23 tested were
218 confirmed in extended 8 x 8 checkerboard benchmarking assays (9 of which in both *S. aureus*
219 strains) (**Supplementary Table 2**). Interestingly, adjuvants, like clavulanic acid, or antibiotics
220 used in clinics only in fixed-concentration combinations (trimethoprim and sulphonamides),
221 exhibited a number of synergies with other drugs, unveiling a so-far unexplored space for new
222 combinations. We validated the efficacy of one of these combinations (teicoplanin-
223 trimethoprim) against several MRSA clinical isolates in vitro (**Fig. 2d, Extended Data Fig. 7b**)
224 and in vivo in a *G. mellonella* infection model (**Fig. 2e**).

225

226 **Fundamental differences for target-specific synergies between Gram-positive and**
227 **Gram-negative species**

228 Drugs belonging to the same class or targeting the same cellular process exhibited mainly
229 synergistic interactions in all three species (**Fig. 2a-b, Extended Data Fig. 5, 8a**). Indeed,
230 synergies between drugs targeting the same process were significantly enriched (**Fig. 3a**), in
231 agreement with previous data on Gram-negative bacteria¹. Targeting different facets of the
232 same cellular process can bypass the inbuilt redundancy and robustness of biological
233 processes³⁴. Importantly, the targeted cellular processes that were more prone to synergies
234 were distinct when comparing Gram-positive and Gram-negative species (**Extended Data**
235 **Fig. 8a-b**). Synergies between protein-synthesis inhibitors were specifically prevalent in
236 Gram-positive species, whereas Gram-negative species were dominated by synergies
237 between cell-wall inhibitors (**Fig. 3b, Extended Data Fig. 8c-f**). Since the drugs between the
238 two screens largely overlapped, and their targets are conserved in bacteria, we decided to
239 further investigate the underlying reason for this clear difference.

240

241 Protein-synthesis inhibitors are mostly used against Gram-positive bacteria, as they often
242 cannot cross the outer membrane (OM) of Gram-negative bacteria. We reasoned that in
243 Gram-positive species, with no such permeability bottleneck, these drugs could synergize at
244 their target level – the ribosome, as shown before by combinations of genetic perturbations of
245 translation³⁵. By contrast, in Gram-negative bacteria the OM permeability bottleneck likely
246 masks such synergistic interactions and enriches for antagonisms, which are often due to a
247 decrease in drug intracellular concentration(s)¹. We confirmed this hypothesis by using the
248 OM-defective *E.coli* mutant *lptD4213*, which is hyperpermeable to hydrophobic antibiotics and
249 detergents^{36,37}. Many of the interactions between macrolides and different classes of protein
250 synthesis inhibitors became synergistic in this *E. coli* mutant background (**Fig. 3c, Extended**
251 **Data Fig. 9**), demonstrating that drug uptake bottlenecks can change antibiotic interactions.
252

253 While fosfomycin- and bacitracin-based interactions are mostly conserved within Gram-
254 positive species and across the Gram-positive/-negative divide, interactions within beta-
255 lactams are radically different between Gram-positive and -negative species, with synergies
256 being rare in the former (**Extended Data Fig. 8e-f, Supplementary Table 3**). Beta-lactams
257 have different affinities to the various penicillin-binding proteins (PBPs) present in bacteria³⁸.
258 Interestingly, the number and type of PBPs are largely different across bacterial species^{38,39},
259 so we hypothesized that this redundancy (number of PBP paralogues) was driving the
260 observed difference. Indeed, the number of synergies in each strain tested correlated with the
261 number of PBPs reported in each species (**Fig. 3d**). The higher the number of PBPs, the
262 higher the probability that combining beta-lactams with different affinities to the various PBPs
263 will lead to a synergistic bypassing of the redundancy. While further studies are needed, we
264 hypothesize that this target redundancy drives the synergies between beta-lactam antibiotics,
265 and that the difference we observed here between Gram-positive and -negative species likely
266 depends on the number of PBPs in the species tested (**Supplementary Table 5**).

267

268 Altogether, these results support the concept that drug interactions mirror key properties of
269 cellular networks, such as their functional modularity and redundancy, and reflect fundamental
270 differences in cellular architecture and physiology across the Gram-positive/-negative divide.
271

272 **An underestimated reservoir of interactions between non-antibiotics and antibiotics**

273 Our drug interaction screen included eight non-antibiotic drugs, which exhibited a similar
274 interaction frequency (11%) as antibiotics (13%) (**Fig. 4a**). This motivated us to expand the
275 panel of non-antibiotic drugs tested, and to explore the range of synergies and antagonisms
276 antibiotics exhibit with commonly used non-antibiotic medications in *S. aureus*. We selected
277 44 drugs to include pharmaceuticals that can be co-administered with antibiotics in *S. aureus*
278 infections or non-antibiotics with previously reported antibacterial activity against *S. aureus*
279 (**Supplementary Table 6**). Altogether, we covered 19 therapeutic classes (**Fig. 4d**,
280 **Supplementary Table 6**), testing each drug in a range of three concentrations and against
281 the panel of 62 drugs of the initial screen (2728 drug-drug interactions, 4 x 4 dose matrix) in
282 *S. aureus* DSM 20231. Concentrations were selected to fall within therapeutic plasma
283 concentrations⁴⁰, except for drugs with possible topical use, where higher concentrations were
284 used. Interactions were scored and benchmarked as for the main screen (Methods,
285 **Supplementary Table 6, Extended Data Fig. 10a-d**).

286

287 We confidently detected 197 interactions in the extended screen (**Fig. 4b, Supplementary**
288 **Table 6**), an interaction frequency that was lower (7.8%) than the one of the initial screen or
289 the set of eight non-antibiotic drugs included therein (**Fig. 4a**). Since all eight non-antibiotic
290 drugs included in the main screen were selected because they had reported antibacterial
291 activity, we reasoned that this could account for their higher interaction rate. Indeed, for those
292 drugs that had antibacterial activity on their own, the interaction frequency was double (12%
293 as compared to 5.9%) (**Fig. 4c**). For all non-antibiotics tested in this work (n = 52), we detected
294 140 synergies and 105 antagonisms mainly with antibiotics (**Fig. 4d**). A small number of
295 interactions (22 synergies and 23 antagonisms) were found between two non-antibiotics.

296 Synergies offer a so-far unexploited potential for drug repurposing, whereas antagonisms
297 expose risks of decreasing the efficacy of antimicrobial treatments.

298

299 The therapeutic classes that exhibited the highest number of interactions were anti-
300 inflammatory drugs ($n = 7$, of which four NSAIDs) and hormone analogues ($n = 6$) (**Fig. 4d**,

301 **Extended Data Fig. 10e, Supplementary Table 6**), whereas in terms of antibiotics, protein-
302 synthesis inhibitors dominated the interactions (**Fig. 4d, Extended Data Fig. 10f**,

303 **Supplementary Table 6**). Interestingly, selective estrogen-receptor modulators (SERMs),
304 such as the two triphenylethylene compounds tamoxifene and clomifene, shared their

305 synergies with cell-wall acting drugs and their antagonism with streptomycin. Hormone

306 analogues engaged in several synergies ($n = 11$) and antagonisms ($n = 17$), suggesting an
307 understudied impact that such commonly-used drugs, and potentially their natural

308 counterparts, may have on the efficacy of antibacterial therapies^{14,41}. For the anti-inflammatory

309 drugs, only four interactions with acetylsalicylic acid were previously known: its synergy with
310 cefuroxime⁴² and its antagonisms with ciprofloxacin, oxacillin and azithromycin^{43–45}. We

311 validated the synergy between ibuprofen and gentamicin also against MRSA clinical isolates,

312 including a strain resistant to linezolid (a last-resort antibiotic for MRSA), in vitro and in vivo in

313 a *G. mellonella* infection model (**Fig. 4e-f, Extended Data Fig. 11**).

314

315 **The antiaggregant ticagrelor has a broad impact on *S. aureus* physiology that accounts**
316 **for its promiscuous interactions with antibiotics**

317 Ticagrelor, a purine analogue antiaggregant acting on the adenosine P2Y₁₂ receptor⁴⁶, had
318 the highest number of interactions ($n = 27$) among the 44 non-antibiotics tested (**Fig. 4d**).

319 Ticagrelor has been shown to improve clinical outcomes in patients with pneumonia and
320 sepsis caused by Gram-positive bacteria^{47,48}. This effect has been supported by different

321 degrees of evidence that ticagrelor activates platelets upon systemic infection⁴⁸, protects them
322 from *S. aureus* toxin-mediated damage⁴⁹, modulates their antibacterial properties⁵⁰, and exerts

323 a direct bactericidal activity on *S. aureus* at very high concentrations⁵¹. However, the mode of

324 action of ticagrelor on *S. aureus* and its interactions with other drugs have remained largely
325 uncharacterised.

326

327 To gain insights into the mode of action and interaction of ticagrelor, we used two-dimensional
328 thermal proteome profiling (2D-TPP)^{52–54} in both lysate and whole cell samples to investigate
329 the direct and indirect effects of the drug, respectively (Methods). We observed a
330 destabilisation of a number of ATP- and GTP-binding enzymes and transporters in both the
331 whole cell and the lysate (**Fig. 5a-b, Extended Data Fig. 12a, Supplementary Table 7**), and
332 the induction of many purine biosynthesis enzymes (PurC, PurD, PurE, PurF, PurH, PurK,
333 PurL, PurM, PurN, PurQ) in live cells (**Fig 5a, Extended Data Fig. 12a-b**). This is in agreement
334 with ticagrelor being a purine analogue. Furthermore, the MIC of ticagrelor increased upon
335 supplementation of defined media with adenosine, inosine or their combination (**Extended**
336 **Data Fig. 12c**), suggesting that ticagrelor interferes with purine metabolism in *S. aureus*.

337

338 As mentioned above, the clinically observed effects of ticagrelor during *S. aureus* infection
339 have not been linked so far to a direct effect of ticagrelor on *S. aureus* virulence. We
340 discovered a pervasive impact of ticagrelor on *S. aureus* virulence determinants and
341 regulators, many of which were down-regulated, and others destabilized (**Fig 5a, Extended**
342 **Data Fig. 12a, Supplementary Table 7**). In particular, we observed destabilisation in lysate
343 and downregulation in whole-cell samples of key clotting factors secreted by *S. aureus* (ClfA,
344 ClfB), the coagulase Coa and the von Willebrand-factor binding protein (vWBP)
345 NWMN_0757⁵⁵. These effects, evident at a clinically-relevant ticagrelor concentration⁵¹ offer
346 an alternative explanation for the beneficial effect of antiaggregant therapy as an adjuvant in
347 *S. aureus* systemic infection.

348

349 Ticagrelor exhibited a number of synergies and antagonisms with antibiotics in MSSA
350 (Methicillin-sensitive *S. aureus*; **Fig. 4d**). Interestingly, it broadly sensitized MSSA and MRSA
351 to both cationic peptides (nisin; **Extended Data Fig. 12d**) and antibiotics (aminoglycosides,

such as gentamicin; **Fig. 5c, Extended Data Fig. 11**). This potentiation effect of aminoglycosides occurred at low ticagrelor concentrations, and was also evident at the killing level (**Fig. 5d**) and *in vivo*, during infection of *G. mellonella* (**Fig. 5e**). Since aminoglycosides need energy to cross the membrane in most bacteria⁵⁶, we wondered whether ticagrelor acted at that level, for example by modulating the cell surface charge and increasing aminoglycoside uptake. Consistent with this hypothesis, two proteins involved in the lipoteichoic acid (LTA) D-alanylation⁵⁷, DltC and DltD, were destabilized in the TPP lysate data, and TagG, a subunit of the cell wall teichoic acid (WTA) translocase, was destabilised in the whole cell sample (**Fig 5a-b, Extended Data Fig. 12e**). Disruption of teichoic acids, and specifically, inactivation of *dltA*, *dltB* and *dltC* have been shown to sensitize *S. aureus* to cationic compounds because of an increase in the net negative charge of *S. aureus* surface⁵⁸⁻⁶⁰. We observed a decrease in the MIC of the aminoglycoside gentamicin and the cationic antibiotic nisin in IPTG-inducible CRISPRi knockdown mutants of both the *dltABCD* operon and of *tagG* (Methods, **Fig. 5f, Extended Data Fig. 12f**). Ticagrelor treatment also increased the binding of positively-charged cytochrome C to intact *S. aureus* cells (**Fig. 5g, Extended Data Fig. 12g-h**). Thus, ticagrelor treatment impacts the thermal stability and presumably the activity of proteins involved in WTA flipping and LTA D-alanylation, leading to an increase in the surface net negative charge of *S. aureus*. This leads to potentiation of the uptake of cationic antibiotics, such as aminoglycosides and nisin.

371

372 Discussion

373 In this study, we have systematically profiled drug combinations in three prominent Gram-
374 positive bacterial species. We probed multiple compounds from each of the main antibiotic
375 classes used to treat infections caused by Gram-positive pathogens, as well as neglected
376 antibiotics, commonly used antibiotic adjuvants, and promising non-antibiotic drugs with
377 reported antibacterial activity. In all cases combinations were tested in a dose-dependent
378 manner and interactions were assessed in a quantitative manner. This effort unravelled a

379 plethora of interactions, the majority of which have not been previously not reported. A number
380 of the synergies that we discovered using lab strains were also effective against MDR clinical
381 isolates and during infections *in vivo*. Overall, the data generated here can seed future
382 experiments to mechanistically dissect key interactions or to explore their potential for clinical
383 application. For example, some of the synergies and antagonisms identified may guide future
384 broad-spectrum empiric treatments – i.e. when antibiotic regimens are started without
385 knowledge of the responsible pathogen in time-sensitive contexts (e.g. sepsis). Fosfomycin
386 synergies that are strong and conserved across the Gram-positive/-negative divide are good
387 candidates, as fosfomycin is increasingly used in clinics⁶¹, but rarely in combinations. To
388 enable further use of this rich resource, we made all data browsable in a user-friendly interface.
389

390 A previous large-scale study from our group in three Gram-negative species¹ enabled
391 important comparative insights across the Gram-positive/-negative divide. The confidence and
392 depth level of these comparisons are high, since the two studies have similar experimental
393 and data analysis design (including the drugs tested). As in Gram-negative species, drug
394 interactions are largely species-specific with synergies tending to be more conserved and
395 driven by antibiotics sharing general cellular targets. Only a small number of interactions is
396 conserved across Gram-positive and -negative species. Differences in the cell surface
397 organization (e.g. the outer membrane posing a permeability barrier for hydrophobic
398 compounds) or in the degree of redundancy in cell-wall building enzymes can explain some
399 of the strong synergies observed specifically in Gram-positive or Gram-negative species.
400

401 We also attempted to leverage the adjuvant potential of approved non-antibiotic drugs by
402 probing a large number of combinations with antibiotics (2728) in a dose-dependent manner
403 in *S. aureus*. Although the interaction potential was lower for drugs without antibacterial
404 activity, the room for novelty is high with the vast majority of synergies detected being
405 previously unknown. While non-antibiotic drugs have been proposed as anti-infective
406 adjuvants for decades^{5,6}, the *in vivo* relevance and molecular basis of their antibacterial action

407 is known only for a few examples^{6,8,18,51,62,63}. Here we further studied the antiaggregant
408 ticagrelor, whose repurposing as an anti-infective adjuvant for Gram-positive bacteria has
409 been recently proposed^{49,64}. While the *in vivo* benefit of ticagrelor for systemic infections has
410 been documented^{47,51}, we exposed here a large number of additional synergies with antibiotics
411 in *S. aureus* (n = 13), and provided molecular insights into how ticagrelor affects *S. aureus*
412 physiology and potentiates the activity of positively-charged antibiotics, such as
413 aminoglycosides or nisin.

414

415 Drugs are regularly combined in clinics not only in rationally designed therapeutic schemes,
416 but also extemporarily in poly-treated patients¹⁴. Although interactions at the host
417 pharmacokinetic level are routinely avoided, it is assumed that interactions at the bacterial
418 level would not affect overall anti-infective efficacy. In addition to synergies, we detected an
419 equally large number of antagonisms between commonly administered non-antibiotic drugs
420 and antibiotics. Such antagonisms could decrease the efficacy of the antibiotic treatment and
421 increase the probability of resistance emergence for the antibiotic. Overall, it is important to
422 start assessing drug interactions not only at the level of growth inhibition, but also at the level
423 of killing and ultimately clearing of the infection, as the outcome of interactions may differ¹¹.

424

425 It has also been recently proposed that the attenuation of antibiotic efficacy (antagonism) can
426 be used to decrease the spectrum and collateral damage of antibiotics to commensal
427 bacteria⁶⁵. In our screen, loperamide had the highest number of interactions with antibiotics.
428 Although its potential use as adjuvant for specific antibiotics and its mode-of-action are
429 known⁶, we could detect an additional broad antagonism with macrolides. Loperamide and
430 macrolides are often co-administered for travellers' diarrhoea⁶², which is caused by Gram-
431 negative enteric pathogens. It is tempting to speculate that part of the beneficial effect of the
432 combination could also lie in the protection of Gram-positive commensal gut species from
433 macrolides.

434

435 In summary, we present a systematic and quantitative account of drug interactions in key
436 Gram-positive species, discovering a number of potent synergies that are effective against
437 clinical MDR isolates, and providing insights into the underlying mechanisms of some of the
438 observed interactions. In an era where novel antibiotic development faces technical and
439 economic hurdles, and new antimicrobial strategies are urgently needed, systematic drug
440 interaction profiling can offer possible solutions to treat bacterial infections. Extending the
441 systematic testing of drug interactions to more bacteria and to other types of non-antibiotic
442 drugs will improve our understanding of drug interaction conservation and mechanisms, and
443 potentially inform tailored treatments towards pathogens.

444 **Materials and methods**

445 **Strains and growth conditions**

446 All strains used in this study are listed in **Supplementary Table 1**. *B. subtilis* subsp *subtilis*
447 168⁶⁶ was kindly provided by Carol A. Gross, all MRSA clinical isolates by Stephan Göttig, S.
448 *pneumoniae* D39V⁶⁷ by Jan-Willem Veening, and *S. aureus* USA300 by Daniel Lopez.
449 *Staphylococcus aureus* subsp *aureus* Newman⁶⁸ was purchased from NCTC (NCTC 8178).
450 and DSM 20231⁶⁹ (ATCC 12600^T, NCTC 8532) from DSMZ, Braunschweig, Germany.

451

452 For all experiments and unless otherwise specified, *S. aureus* strains were grown in Tryptic
453 Soy Broth (TSB, ref. 22092 by Merck-Millipore), *B. subtilis* was grown in LB Lennox, and *S.*
454 *pneumoniae* was grown in CY medium, adapted from⁷⁰. All species were grown at 37°C, with
455 vigorous shaking (850 rpm), except for *S. pneumoniae*, which was grown without shaking. The
456 ticagrelor purine supplementation experiments in *S. aureus* Newman were conducted in
457 SSM9PR defined medium supplemented with 1% glucose⁷¹.

458

459 **Inducible knockdown strain construction**

460 A two-plasmid CRISPR interference system was used to knock down gene expression of
461 selected genes in *S. aureus* Newman⁷². In these strains, *dcas* is expressed from an IPTG-
462 inducible promoter on plasmid pLOW, while sgRNAs are expressed from a constitutive promoter
463 on a plasmid derived from pCG248. The sgRNA-target sequences were
464 TGTCTAACAGCAATGCTTG for *dltABCD* and AAACCATAATTGCATAACA for *tagG*, and
465 ATAGAGGATAGAATGGCGCC for the non-target control MM76 (**Supplementary Table 1**).
466

467 **MIC determination**

468 MICs were tested in all strains for the main screen (**Supplementary Table 1**). Drugs were
469 two-fold serially diluted in 11 concentrations, and 32 no-drug control wells were included in
470 each plate. Experiments were conducted in flat, clear-bottom 384 well plates (ref. 781271 by

471 Greiner BioOne), with a total volume of 30 µl for *S. aureus* and *B. subtilis* and 55 µl for *S.*
472 *pneumoniae*. Volumes were optimised for each strain to achieve good dynamic range for
473 growth and minimize risk of cross-contamination between wells. Plates were inoculated with
474 a starting optical density at 595 nm (OD_{595nm}) of 0.01 from an overnight culture. All liquid
475 handling was performed using a Biomek FX liquid handler (Beckman Coulter). Plates were
476 sealed with breathable membranes and incubated at 37°C. OD_{595nm} was measured every 30
477 minutes for 14 hours. The MIC was considered as the first concentration at which growth was
478 inhibited. Experiments were conducted in biological duplicates. For the adjuvant screen,
479 antibiotics were tested in *S. aureus* DSM 20231 at the same concentrations as for the main
480 screen. Non-antibiotics concentrations were selected to fall within therapeutic plasma
481 concentrations⁴⁰(**Supplementary Table 6**).

482

483 **High-throughput screen of drug combinations**

484 Sixty-two drugs, hereafter designated as recipients, were arrayed in flat, clear-bottom 384-
485 well plates in three two-fold serial dilutions and two technical replicates – up to two recipient
486 drugs were removed from the data of the different strains due to quality control reasons.
487 Concentrations were selected according to MICs, with the highest concentration
488 corresponding to the MIC, and the intermediate and lowest concentration corresponding to
489 half and a quarter of MIC, respectively (**Supplementary Table 1**). Plates were kept frozen
490 and defrosted upon each experimental run, when the same 62 drugs and in the same three
491 concentrations were added as donor drugs (one drug at one concentration for each recipient
492 plate). A few drugs were screened only as donors: the combinations co-amoxiclav and
493 cotrimoxazole in *B. subtilis* and *S. aureus* DSM 20231; co-amoxiclav, clavulanic acid,
494 pseudomonic acid and cefuroxime in *S. aureus* Newman. All donor drugs were tested in two
495 biological replicates. Control wells were included in each plate (six no-drug wells, three plain
496 medium wells and three wells containing only the donor drug). After the addition of donor
497 drugs, plates were inoculated with cells. Handling, inoculation, growth conditions, plate
498 incubation and OD_{595nm} measurements were performed as for the MIC determination.

499 For the adjuvant screen, 44 non-antibiotic drugs (**Supplementary Table 6**) were tested
500 against the same 62 recipient drugs of the main screen for *S. aureus* DSM 20231.

501

502 **Screen benchmarking and 8 x 8 checkerboard assays**

503 Combinations were tested in the same experimental conditions as for the screen, but at higher
504 concentration resolution. Drugs were diluted in eight concentrations spanning linearly-space
505 gradients to assemble 8 x 8 checkerboards for each combination tested – highest
506 concentration used can be found in **Supplementary Table 2**. All experiments were conducted
507 in at least two technical and two biological replicates. Data was analysed with the same
508 pipeline as for the screen (Methods).

509

510 **Data analysis**

511 Data analysis was adapted from¹. Growth curves were processed as described in **Extended**
512 **Data Fig. 1**: the background was subtracted from all OD_{595nm} measurements, on a well-by-well
513 basis using the first measurement obtained. Abnormal spikes in OD values of the first three
514 time points occurred in *S. pneumoniae* in a small fraction of wells due to bubble formation in
515 the medium or plate condensation. These early local peaks in OD curves were identified and
516 replaced with the median of OD values (of corresponding time points) estimated from the wells
517 not affected by such artefacts within the same plate. When more than one in the first four time
518 points was affected, those wells were identified as non-monotonically-increasing OD_{595nm}
519 values across the first four time points, and their background was estimated as the median
520 first-time-point OD_{595nm} of artefact-free wells (monotonically increasing across the first four
521 time points).

522

523 The time point corresponding to the transition between exponential and stationary phase in
524 no-drug control wells was identified as the first time point at which the maximum OD_{595nm} was
525 reached. This time point was selected according to the growth characteristics of each strain,
526 and was kept the same across runs: 8 h for both *S. aureus* strains, 5.5 h for *B. subtilis* and 3.7

527 h for *S. pneumoniae*. Later time points were excluded from further analysis. The OD_{595nm}
528 measurement at that time point was used to derive fitness measurements that captured effects
529 both on growth rate and maximum yield. OD-based endpoints correlated well with AUC-based
530 endpoints (Pearson correlation 0.95), and led to higher precision and recall according to the
531 screen benchmarking (**Extended Data Fig. 2d-e**).

532

533 This value was then divided, per plate, by the robust mean⁷³ of the six no-drug controls (no-
534 drug control hereafter), obtaining three fitness measures for each drug concentration pair: f_1 ,
535 fitness upon exposure to drug 1; f_2 , fitness upon exposure to drug 2; and $f_{1,2}$, fitness in
536 presence of drug 1 + drug 2. Based on these values, further quality control was again
537 performed, correcting fitness increase artefacts (maximum fitness was set to 1) and removing
538 plates with poor technical replicate correlation (Pearson correlation < 0.7). f_1 , f_2 , and $f_{1,2}$ were
539 used to calculate interaction scores using the Bliss model¹⁹. The choice of this model over
540 other available quantification methods was driven by the following considerations: (i) the three
541 measurements obtained for drug dose responses are not sufficient for accurate quantification
542 using alternative models (e.g. the Loewe model⁷⁴) and (ii) the Bliss model can more accurately
543 account for single drugs with no effect (such as most non-antibiotic drugs included in the
544 screen).

545

546 Bliss (ε) scores were calculated as follows:

547

548 [eq.1]
$$\varepsilon = f_{d1,d2} - f_{d1} * f_{d2}$$

549

550 where $f_{d1,d2}$ corresponds to the observed fitness in the presence of the drug combination, and
551 f_{d1} and f_{d2} correspond to the fitness in the presence of the two single drugs.

552

553 Single drug fitness for both donor and recipient drugs can also be inferred from combination
554 fitness, by minimizing the sum of residuals squared of the Bliss independence model as
555 follows and using the assumption that most drugs interact neutrally:
556 [eq.2]

557
$$\{f_{d1}, f_{d2}\} = \arg \min_{d1, d2} \|f_{d1, d2} - f_{d1} * f_{d2}\|^2$$

558
559 Experimentally measured and estimated fitness values were very similar for donor (**Extended**
560 **Data Fig. 2f**) and recipient (**Extended Data Fig. 2g**) drugs, and we used the estimated
561 measures since those were more robust to noise - experimental controls were limited for donor
562 drugs (three single-drug control wells) and sometimes biased for recipient drugs, as a single
563 problematic plate in the batch was sufficient to generate noise.

564
565 When no data was discarded upon quality control, the number of Bliss scores obtained for
566 each combination was 72, composed of 3 x 3 (in the two-dimensional concentration space) x
567 two technical replicates x two biological replicates x two replicates with drugs tested as donor
568 or recipient. Hit calling was performed using a resampling procedure with 10,000 repetitions
569 for each combination tested, where the ε distribution for each combination was compared with
570 the resampled Bliss scores using Wilcoxon rank-sum test in each iteration¹. Hits correspond
571 to combinations with FDR < 0.05.

572
573 As before¹, we coupled this significance threshold to an effect-size threshold. For each
574 combination we defined a cumulative score using the quartiles of its distribution of ε scores.
575 We tested the performance of different thresholds in precision and recall upon screen
576 benchmarking, and identified |0.1| as best threshold, with precision 0.87 and recall 0.68
577 (**Extended Data Fig. 3d**). Accordingly, synergies were assigned if the first quartile of the ε
578 distribution < -0.1 and antagonisms if the third quartile exceeded 0.1. We could increase the

579 screen recall by leveraging the presence of two strains belonging to the same species in the
580 case of *S. aureus*, as previously described for Gram-negative species¹. We defined an
581 additional set of hits (weak and conserved), meeting significance and effect size thresholds in
582 one strain, but with lower effect size in the other strain. A cutoff of |0.08| allowed us to maintain
583 the same precision and increase the recall to 0.72.

584

585 Data analysis was implemented with R v.4.1.2⁷⁵ and RStudio v.2021.09.1⁷⁶ and networks were
586 created with Cytoscape v.3.8.2⁷⁷.

587

588 **Interaction detection calculation**

589 Interaction detection rates were calculated by dividing the number of detected interactions by
590 the number of combinations for which interactions could be observed according to the mapped
591 fitness space¹. Synergies could not be observed when the expected fitness of a drug
592 combination (defined as the product of single-drug fitness values in eq. 1) was lower than 0.1,
593 while antagonisms could not be detected for expected combination fitness higher than 0.9 (2.1
594 and 3.3% of the 7986 combinations tested, respectively).

595

596 **Drug clustering**

597 Drug-drug interaction profiles were clustered according to the cosine similarity of quartile-
598 based Bliss interaction scores of each drug pair in each strain. Scores from all interactions
599 were considered, regardless of their statistical significance. For the clustering based on
600 chemical structures, drugs were clustered according to their Tanimoto similarity⁷⁸ using 1024-
601 bit ECFP4 fingerprints⁷⁹.

602

603 **Phylogeny analysis**

604 To calculate the percentage sequence identity between bacterial species, the genomes of *B.*
605 *subtilis* 168, *S. aureus* Newman, *S. aureus* DSM 20231, *S. pneumoniae* D39, *E. coli* K-12, *S.*
606 *enterica* serovar Typhimurium LT and *P. aeruginosa* PAO1 were downloaded from NCBI and

607 40 universal single-copy marker genes (MGs) were extracted using the fetchMG script⁸⁰. The
608 40 MGs were selected from a previous publication for their ability to characterise
609 prokaryotic species²¹, and they encode for ubiquitous functions like tRNA synthetases or are
610 ribosomal proteins (EggNOG COGs: COG0012, COG0016, COG0018, COG0048, COG0049,
611 COG0052, COG0080, COG0081, COG0085, COG0087, COG0088, COG0090, COG0091,
612 COG0092, COG0093, COG0094, COG0096, COG0097, COG0098, COG0099, COG0100,
613 COG0102, COG0103, COG0124, COG0172, COG0184, COG0185, COG0186, COG0197,
614 COG0200, COG0201, COG0202, COG0215, COG0256, COG0495, COG0522, COG0525,
615 COG0533, COG0541, COG0552). The concatenated sequences (all six genomes contained
616 exactly 40 MGs) were used to calculate percentage nucleotide sequence identity with
617 vsearch⁸¹ and to create a phylogenetic tree. To this end, a multiple sequence alignment was
618 created with muscle v3.8.1551⁸² with default parameters. Finally, a maximum-likelihood
619 phylogenetic tree was constructed using the online tool PhymL 3.0⁸³ with default parameters.
620 To evaluate interaction conservation, only the 46 drugs tested both in Gram-positive and
621 Gram-negative species (**Supplementary Table 1**) were considered.

622

623 **Evaluation of drug combination therapy using the *G. mellonella* infection model**

624 Larvae of the greater wax moth (*Galleria mellonella*) at their final instar larval stage were used
625 for evaluation of selected drug combinations to assess their efficacy against MRSA *in vivo*.
626 Larvae were purchased from UK Waxworms (Sheffield, UK) and Mucha Terra (Ahaus-
627 Altstätte, Germany). Stock solutions of cefepime, gentamicin, ibuprofen, teicoplanin and
628 trimethoprim were freshly prepared as described for the *in vitro* experiments (**Supplementary**
629 **Tables 1, 6**) with the exception of ticagrelor which was dissolved in 50 mM EtOH and diluted
630 in distilled water to the required concentration. Drug toxicity was preliminarily assessed
631 injecting larvae with serial dilutions of single drugs and combinations. Concentrations at which
632 no toxicity was observed were selected for further experiments. The MRSA strains were
633 cultivated in brain heart infusion medium and harvested at an OD₆₀₀ of 0.5. Bacteria were
634 washed twice with PBS and adjusted to an OD₆₀₀ which corresponded to a lethal dose of

635 approximately 75% (LD₇₅) of the larvae after 24 h (approximately 10⁷ CFUs). Ten larvae per
636 condition were injected with 10 µL of the bacterial cell suspension or PBS (referred to as
637 uninfected control) into the hemocoel via the last left proleg using Hamilton precision syringes.
638 After one hour, 10 µL of single drugs combinations, or vehicle were injected into the last right
639 proleg, at the following drug concentrations: teicoplanin 1 µg/ml, trimethoprim 250 µg/ml,
640 cefepime 0.025 µg/ml, gentamicin 2 µg/ml, ibuprofen 4 µg/ml, ticagrelor 100 µg/ml. The
641 survival of *Galleria* larvae was monitored at the indicated time points by two observers
642 independently. Each strain–drug combination was evaluated in three independent
643 experiments.

644

645 **Time-kill experiments**

646 Overnight cultures of *S. aureus* USA300 were diluted 1:100 in 20 ml of TSB medium, incubated
647 for 1h in flasks at 37°C with continuous shaking and diluted again 1:100 in 20 ml prewarmed
648 TSB with ticagrelor (5 µg/ml), gentamicin (1.5 µg/ml), their combination or without drugs. 50 µl
649 of serial 10-fold dilutions of cultures were plated on TSA plates every 30 minutes for 2 hours.
650 Cell viability was determined by counting CFUs after plates were incubated overnight in four
651 independent experiments.

652

653 **Two-dimensional thermal proteome profiling (2D-TPP)**

654 Bacterial cells were grown overnight at 37°C in TSB and diluted 1000-fold into 50 ml of fresh
655 medium. Cultures were grown at 37°C with shaking until OD₅₇₈ ~0.6. Ticagrelor at the desired
656 concentrations (0.04, 0.16, 0.8 and 4 µg/ml) or a vehicle-treated control were added and
657 cultures were incubated at 37°C for 10 minutes. Cells were then pelleted at 4,000 x g for 5
658 min, washed with 10 ml PBS containing the drug at the appropriate concentrations,
659 resuspended in the same buffer to an OD₅₇₈ of 10 and aliquoted to a PCR plate. The plate
660 was then exposed to a temperature gradient for 3 min in a PCR machine (Agilent SureCycler
661 8800), followed by 3 min at room temperature. Cells were lysed with lysis buffer (final
662 concentration: 50 µg/ml lysostaphin, 0.8% NP-40, 1x protease inhibitor (Roche), 250 U/ml

663 benzonase and 1 mM MgCl₂ in PBS) for 20 min, shaking at room temperature, followed by
664 five freeze–thaw cycles. Protein aggregates were then removed by centrifuging the plate at
665 2,000 × g and filtering the supernatant at 500 × g through a 0.45 µm filter plate for 5 minutes
666 at 4°C. Protein digestion, peptide labelling, and MS-based proteomics were performed as
667 previously described⁵³.

668

669 **2D-TPP data analysis**

670 Data were pre-processed and normalized as previously described⁵². Peptide and protein
671 identification were performed against the *S. aureus* Newman strain Uniprot FASTA (Proteome
672 ID: UP000006386), modified to include known contaminants and the reversed protein
673 sequences. Data analysis was performed in R using the package TPP2D⁸⁴ as previously
674 described⁸⁵. Briefly, to identify stability changes, a null model, allowing the soluble protein
675 fraction to depend only on temperature, and an alternative model, corresponding to a
676 sigmoidal dose-response function for each temperature step, are fitted to the data. For each
677 protein the residual sum of squares (RSS) of the two models are compared to obtain an F-
678 statistic. FDR control is performed with a bootstrap procedure as previously described⁸⁵. The
679 abundance or thermal stability effect size was calculated for each protein as following:

680

681 [eq.3]
$$\text{sign}(\kappa) \cdot \sqrt{\text{RSS}^0 - \text{RSS}^1}$$

682

683 where κ is the slope of the dose-response model fitted across temperatures and drug
684 concentrations and RSS⁰ and RSS¹ correspond to the residual sum of squares of the null
685 (pEC50 linearly scaling with temperature) and alternative model, respectively⁸⁶.

686

687 **KEGG enrichment**

688 *S. aureus* Newman proteome was annotated using KEGG⁸⁷ (release 100.0, October 1).
689 Proteins with missing KEGG annotation were preliminarily removed. Fisher's exact test was

690 then used to test the enrichment of input protein sets (hits corresponding to FDR < 0.05)
691 against the background (all detected proteins) for each term. The p-values were corrected for
692 multiple testing using the Benjamini-Hochberg procedure. The analysis was performed in R
693 using the packages KEGGREST⁸⁸, EnrichmentBrowser⁸⁹ and clusterProfiler⁹⁰.

694

695 **Ticagrelor MIC upon purine depletion and supplementation**

696 Ticagrelor (ref. SML2482, Sigma-Aldrich) MIC was measured upon purine supplementation in
697 *S. aureus* Newman as described above in SSM9PR defined medium supplemented with 1%
698 glucose⁷¹, in flat, clear-bottom 384-well plates with a final volume of 30 µl. Adenine and inosine
699 were added at 20 and 100 µg/ml or in combination, both at 100 µg/ml. Experiments were
700 conducted in four biological replicates. A single time-point OD_{595nm} at the transition between
701 exponential and stationary phase (13.5 h) was used to derive dose-response curves, after
702 normalisation to the respective no-drug control for each condition.

703

704 **Gentamicin and nisin MIC measurements in *dltABCD* and *tagG* knockdown mutants**

705 For gentamicin and nisin MIC measurements, *dltABCD* and *tagG* IPTG-inducible knockdown
706 mutants (Methods, **Supplementary Table 1**) were grown in two-fold dilutions of nisin and
707 gentamicin, in presence of erythromycin (5 µg/ml) and chloramphenicol (10µg/ml) for plasmid
708 maintenance. IPTG (500 µM) was used to achieve maximal dCas9 expression and thereby,
709 knockdown of the gene targeted. The parent *S. aureus* Newman and the control strain MM76
710 (containing the two vectors with dCas9 and a non-targeting sgRNA) were included in all
711 experiments, and experiments were conducted in four biological replicates in 384-well plates.
712 For each plate, we identified the time point where the control strain MM76 (in presence of
713 erythromycin, chloramphenicol and IPTG at the above-mentioned concentrations) reached
714 plateau, defined as the first time point before no increase was detected in log₁₀(OD_{595nm}) values
715 of two consecutive time points. This time point was then used for all wells to derive dose-
716 response curves, after normalisation to the respective no-drug control for each strain and
717 biological replicate. Full growth curves annotated with the time point used for the dose-

718 response curves and dose-response curves with all controls are included in the
719 **Supplementary File.**

720

721 **Determination of cell surface charge**

722 The cytochrome c binding assay was conducted as previously described⁹¹. Briefly, overnight
723 cultures of *S. aureus* Newman were diluted 1:1000 in 20 ml of TSB medium, and grown in
724 flasks at 37°C with continuous shaking until they reached OD_{578nm} ~ 0.45. Samples were then
725 incubated in the same conditions with or without 10 and 5 µg/ml ticagrelor for 20 minutes.
726 Samples were centrifuged at 10000 g for 15 minutes at room temperature, washed twice with
727 20 mM MOPS buffer (pH 7) and concentrated to reach a final A₅₇₈ of 10 in a 96 well-plate (ref.
728 4483481, Applied Biosystems™) containing cytochrome c (0.25 mg/ml, ref. 101467, MP Bio)
729 or MOPS buffer (**Fig. 5g**). The plate was incubated in the dark at room temperature for 10
730 minutes. The cell pellets were collected, and the amount of cytochrome c in the supernatant
731 was determined spectrophotometrically at an OD_{410nm}. Two-fold dilutions of cytochrome c in
732 the same plate, starting from 256 µg/ml, were used to obtain a standard curve onto which a
733 linear model was fitted to calculate cytochrome c concentrations in the other wells. Results
734 are expressed as unbound cytochrome c fraction in the supernatants. Experiments were
735 conducted in four biological replicates.

736

737 **Data and code availability**

738 Drug combination data and the computational pipeline are available on Github:
739 <https://github.com/vladchimescu/comBact>.

740 An interactive interface to navigate the screen data is available
741 (<https://apps.embl.de/combact/>).

742 The mass spectrometry proteomics data have been deposited to the ProteomeXchange
743 Consortium via the PRIDE partner repository with the dataset identifier PXD036188.

744

745 **References**

- 746
- 747 1. Brochado, A. R. *et al.* Species-specific activity of antibacterial drug combinations. *Nature*
748 **559**, 259–263 (2018).
- 749 2. Eliopoulos, GM, Moellering, RC Jr. Antimicrobial combinations. in *Antibiotics in*
750 *Laboratory Medicine, Fourth Edition* (ed. Lorian, V.) 330–396 (Williams & Wilkins, 1996).
- 751 3. Murray, C. J. L. *et al.* Global burden of bacterial antimicrobial resistance in 2019: a
752 systematic analysis. *Lancet* **399**, 629–655 (2022).
- 753 4. Cook, M. A. & Wright, G. D. The past, present, and future of antibiotics. *Sci. Transl. Med.*
754 **14**, eabo7793 (2022).
- 755 5. Tyers, M. & Wright, G. D. Drug combinations: a strategy to extend the life of antibiotics in
756 the 21st century. *Nat. Rev. Microbiol.* **17**, 141–155 (2019).
- 757 6. Ejim, L. *et al.* Combinations of antibiotics and nonantibiotic drugs enhance antimicrobial
758 efficacy. *Nat. Chem. Biol.* **7**, 348–350 (2011).
- 759 7. Taylor, P. L., Rossi, L., De Pascale, G. & Wright, G. D. A forward chemical screen
760 identifies antibiotic adjuvants in *Escherichia coli*. *ACS Chem. Biol.* **7**, 1547–1555 (2012).
- 761 8. Farha, M. A., Verschoor, C. P., Bowdish, D. & Brown, E. D. Collapsing the proton motive
762 force to identify synergistic combinations against *Staphylococcus aureus*. *Chem. Biol.* **20**,
763 1168–1178 (2013).
- 764 9. Farha, M. A. *et al.* Inhibition of WTA synthesis blocks the cooperative action of PBPs and
765 sensitizes MRSA to β-lactams. *ACS Chem. Biol.* **8**, 226–233 (2013).
- 766 10. Campbell, J. *et al.* Synthetic lethal compound combinations reveal a fundamental
767 connection between wall teichoic acid and peptidoglycan biosyntheses in *Staphylococcus*
768 *aureus*. *ACS Chem. Biol.* **6**, 106–116 (2011).
- 769 11. Lázár, V., Snitser, O., Barkan, D. & Kishony, R. Antibiotic combinations reduce
770 *Staphylococcus aureus* clearance. *Nature* **610**, 540–546 (2022).
- 771 12. Jawetz, E. & Gunnison, J. B. Studies on antibiotic synergism and antagonism: a scheme
772 of combined antibiotic action. *Antibiot. Chemother.* **2**, 243–248 (1952).

- 773 13. Roemhild, R., Bollenbach, T. & Andersson, D. I. The physiology and genetics of bacterial
774 responses to antibiotic combinations. *Nat. Rev. Microbiol.* **20**, 478–490 (2022).
- 775 14. Kantor, E. D., Rehm, C. D., Haas, J. S., Chan, A. T. & Giovannucci, E. L. Trends in
776 Prescription Drug Use Among Adults in the United States From 1999-2012. *JAMA* **314**,
777 1818–1831 (2015).
- 778 15. Centers for Disease Control and Prevention (CDC). National Center for Health Statistics
779 (NCHS). National Health and Nutrition Examination Survey Data. Hyattsville, MD: U.S.
780 Department of Health and Human Services, Centers for Disease Control and Prevention,
781 2021, https://www.cdc.gov/nchs/nhanes/2017-2018/p_rxq_rx.htm.
- 782 16. Pai, M. P., Momany, K. M. & Rodvold, K. A. Antibiotic drug interactions. *Med. Clin. North
783 Am.* **90**, 1223–1255 (2006).
- 784 17. Tacconelli, E. *et al.* Discovery, research, and development of new antibiotics: the WHO
785 priority list of antibiotic-resistant bacteria and tuberculosis. *Lancet Infect. Dis.* **18**, 318–
786 327 (2018).
- 787 18. Farha, M. A. *et al.* Antagonism screen for inhibitors of bacterial cell wall biogenesis
788 uncovers an inhibitor of undecaprenyl diphosphate synthase. *Proc. Natl. Acad. Sci. U. S.
789 A.* **112**, 11048–11053 (2015).
- 790 19. Bliss, C. I. THE TOXICITY OF POISONS APPLIED JOINTLY1. *Ann. Appl. Biol.* **26**, 585–
791 615 (1939).
- 792 20. Jawetz, E. The use of combinations of antimicrobial drugs. *Annu. Rev. Pharmacol.* **8**,
793 151–170 (1968).
- 794 21. Mende, D. R., Sunagawa, S., Zeller, G. & Bork, P. Accurate and universal delineation of
795 prokaryotic species. *Nat. Methods* **10**, 881–884 (2013).
- 796 22. Dillon, N. *et al.* Surprising synergy of dual translation inhibition vs. *Acinetobacter
797 baumannii* and other multidrug-resistant bacterial pathogens. *EBioMedicine* **46**, 193–201
798 (2019).
- 799 23. Bollenbach, T., Quan, S., Chait, R. & Kishony, R. Nonoptimal microbial response to
800 antibiotics underlies suppressive drug interactions. *Cell* **139**, 707–718 (2009).

- 801 24. Tang, H.-J. *et al.* Cephalosporin-Glycopeptide Combinations for Use against Clinical
802 Methicillin-Resistant *Staphylococcus aureus* Isolates: Enhanced In vitro Antibacterial
803 Activity. *Front. Microbiol.* **8**, 884 (2017).
- 804 25. Lai, C.-C., Chen, C.-C., Chuang, Y.-C. & Tang, H.-J. Combination of cephalosporins with
805 vancomycin or teicoplanin enhances antibacterial effect of glycopeptides against
806 heterogeneous vancomycin-intermediate *Staphylococcus aureus* (hVISA) and VISA. *Sci.
807 Rep.* **7**, 41758 (2017).
- 808 26. Rieg, S. *et al.* Combination antimicrobial therapy in patients with *Staphylococcus aureus*
809 bacteraemia-a post hoc analysis in 964 prospectively evaluated patients. *Clin. Microbiol.
810 Infect.* **23**, 406.e1-406.e8 (2017).
- 811 27. Leone, S., Noviello, S. & Esposito, S. Combination antibiotic therapy for the treatment of
812 infective endocarditis due to enterococci. *Infection* **44**, 273–281 (2016).
- 813 28. Baddour, L. M. *et al.* Combination antibiotic therapy lowers mortality among severely ill
814 patients with pneumococcal bacteremia. *Am. J. Respir. Crit. Care Med.* **170**, 440–444
815 (2004).
- 816 29. Habib, G. *et al.* 2015 ESC Guidelines for the management of infective endocarditis: The
817 Task Force for the Management of Infective Endocarditis of the European Society of
818 Cardiology (ESC). Endorsed by: European Association for Cardio-Thoracic Surgery
819 (EACTS), the European Association of Nuclear Medicine (EANM). *Eur. Heart J.* **36**, 3075–
820 3128 (2015).
- 821 30. Bartash, R. & Nori, P. Beta-lactam combination therapy for the treatment of
822 *Staphylococcus aureus* and *Enterococcus* species bacteremia: A summary and appraisal
823 of the evidence. *Int. J. Infect. Dis.* **63**, 7–12 (2017).
- 824 31. Ida, T. *et al.* Antagonism between aminoglycosides and beta-lactams in a methicillin-
825 resistant *Staphylococcus aureus* isolate involves induction of an aminoglycoside-
826 modifying enzyme. *Antimicrob. Agents Chemother.* **46**, 1516–1521 (2002).
- 827 32. Vakulenko, S. B. & Mobashery, S. Versatility of aminoglycosides and prospects for their
828 future. *Clin. Microbiol. Rev.* **16**, 430–450 (2003).

- 829 33. Paul, M., Lador, A., Grozinsky-Glasberg, S. & Leibovici, L. Beta lactam antibiotic
830 monotherapy versus beta lactam-aminoglycoside antibiotic combination therapy for
831 sepsis. *Cochrane Database Syst. Rev.* CD003344 (2014).
- 832 34. Typas, A. & Sourjik, V. Bacterial protein networks: properties and functions. *Nat. Rev.*
833 *Microbiol.* **13**, 559–572 (2015).
- 834 35. Kavčič, B., Tkačík, G. & Bollenbach, T. Mechanisms of drug interactions between
835 translation-inhibiting antibiotics. *Nat. Commun.* **11**, 4013 (2020).
- 836 36. Sampson, B. A., Misra, R. & Benson, S. A. Identification and characterization of a new
837 gene of Escherichia coli K-12 involved in outer membrane permeability. *Genetics* **122**,
838 491–501 (1989).
- 839 37. Ruiz, N., Falcone, B., Kahne, D. & Silhavy, T. J. Chemical conditionality: a genetic
840 strategy to probe organelle assembly. *Cell* vol. 121 307–317 (2005).
- 841 38. Sauvage, E., Kerff, F., Terrak, M., Ayala, J. A. & Charlier, P. The penicillin-binding
842 proteins: structure and role in peptidoglycan biosynthesis. *FEMS Microbiol. Rev.* **32**, 234–
843 258 (2008).
- 844 39. Egan, A. J. F., Errington, J. & Vollmer, W. Regulation of peptidoglycan synthesis and
845 remodelling. *Nat. Rev. Microbiol.* **18**, 446–460 (2020).
- 846 40. Schulz, M., Iwersen-Bergmann, S., Andresen, H. & Schmoldt, A. Therapeutic and toxic
847 blood concentrations of nearly 1,000 drugs and other xenobiotics. *Crit. Care* **16**, R136
848 (2012).
- 849 41. Kavanaugh, M. L. & Jerman, J. Contraceptive method use in the United States: trends
850 and characteristics between 2008, 2012 and 2014. *Contraception* **97**, 14–21 (2018).
- 851 42. Chan, E. W. L., Yee, Z. Y., Raja, I. & Yap, J. K. Y. Synergistic effect of non-steroidal anti-
852 inflammatory drugs (NSAIDs) on antibacterial activity of cefuroxime and chloramphenicol
853 against methicillin-resistant *Staphylococcus aureus*. *J Glob Antimicrob Resist* **10**, 70–74
854 (2017).

- 855 43. Zimmermann, P. & Curtis, N. The effect of aspirin on antibiotic susceptibility. *Expert*
856 *Opinion on Therapeutic Targets* vol. 22 967–972 Preprint at
857 <https://doi.org/10.1080/14728222.2018.1527314> (2018).
- 858 44. Cohen, S. P., Levy, S. B., Foulds, J. & Rosner, J. L. Salicylate induction of antibiotic
859 resistance in *Escherichia coli*: activation of the mar operon and a mar-independent
860 pathway. *J. Bacteriol.* **175**, 7856–7862 (1993).
- 861 45. Price, C. T., Lee, I. R. & Gustafson, J. E. The effects of salicylate on bacteria. *Int. J.*
862 *Biochem. Cell Biol.* **32**, 1029–1043 (2000).
- 863 46. Husted, S. & van Giezen, J. J. J. Ticagrelor: the first reversibly binding oral P2Y12
864 receptor antagonist. *Cardiovasc. Ther.* **27**, 259–274 (2009).
- 865 47. Storey, R. F. *et al.* Lower mortality following pulmonary adverse events and sepsis with
866 ticagrelor compared to clopidogrel in the PLATO study. *Platelets* **25**, 517–525 (2014).
- 867 48. Sexton, T. R. *et al.* Ticagrelor Reduces Thromboinflammatory Markers in Patients With
868 Pneumonia. *JACC Basic Transl Sci* **3**, 435–449 (2018).
- 869 49. Sun, J. *et al.* Repurposed drugs block toxin-driven platelet clearance by the hepatic
870 Ashwell-Morell receptor to clear *Staphylococcus aureus* bacteremia. *Sci. Transl. Med.* **13**,
871 (2021).
- 872 50. Ulloa, E. R., Uchiyama, S., Gillespie, R., Nizet, V. & Sakoulas, G. Ticagrelor Increases
873 Platelet-Mediated *Staphylococcus aureus* Killing, Resulting in Clearance of Bacteremia.
874 *J. Infect. Dis.* **224**, 1566–1569 (2021).
- 875 51. Lancellotti, P. *et al.* Antibacterial Activity of Ticagrelor in Conventional Antiplatelet
876 Dosages Against Antibiotic-Resistant Gram-Positive Bacteria. *JAMA Cardiol* **4**, 596–599
877 (2019).
- 878 52. Becher, I. *et al.* Thermal profiling reveals phenylalanine hydroxylase as an off-target of
879 panobinostat. *Nat. Chem. Biol.* **12**, 908–910 (2016).
- 880 53. Mateus, A. *et al.* Thermal proteome profiling in bacteria: probing protein state in vivo. *Mol.*
881 *Syst. Biol.* **14**, e8242 (2018).

- 882 54. Mateus, A. *et al.* Thermal proteome profiling for interrogating protein interactions. *Mol.*
883 *Syst. Biol.* **16**, e9232 (2020).
- 884 55. Cheng, A. G. *et al.* Contribution of coagulases towards *Staphylococcus aureus* disease
885 and protective immunity. *PLoS Pathog.* **6**, e1001036 (2010).
- 886 56. Taber, H. W., Mueller, J. P., Miller, P. F. & Arrow, A. S. Bacterial uptake of aminoglycoside
887 antibiotics. *Microbiol. Rev.* **51**, 439–457 (1987).
- 888 57. Wood, B. M., Santa Maria, J. P., Jr, Matano, L. M., Vickery, C. R. & Walker, S. A partial
889 reconstitution implicates DltD in catalyzing lipoteichoic acid d-alanylation. *J. Biol. Chem.*
890 **293**, 17985–17996 (2018).
- 891 58. Xia, G., Kohler, T. & Peschel, A. The wall teichoic acid and lipoteichoic acid polymers of
892 *Staphylococcus aureus*. *Int. J. Med. Microbiol.* **300**, 148–154 (2010).
- 893 59. Pasquina, L. *et al.* A synthetic lethal approach for compound and target identification in
894 *Staphylococcus aureus*. *Nat. Chem. Biol.* **12**, 40–45 (2016).
- 895 60. Brown, S., Santa Maria, J. P., Jr & Walker, S. Wall teichoic acids of gram-positive bacteria.
896 *Annu. Rev. Microbiol.* **67**, 313–336 (2013).
- 897 61. Sastry, S. & Doi, Y. Fosfomycin: Resurgence of an old companion. *J. Infect. Chemother.*
898 **22**, 273–280 (2016).
- 899 62. Ericsson, C. D., DuPont, H. L., Okhuysen, P. C., Jiang, Z.-D. & DuPont, M. W. Loperamide
900 plus azithromycin more effectively treats travelers' diarrhea in Mexico than azithromycin
901 alone. *J. Travel Med.* **14**, 312–319 (2007).
- 902 63. Miró-Canturri, A., Ayerbe-Algaba, R. & Smani, Y. Drug Repurposing for the Treatment of
903 Bacterial and Fungal Infections. *Front. Microbiol.* **10**, 41 (2019).
- 904 64. Phanchana, M. *et al.* Repurposing a platelet aggregation inhibitor ticagrelor as an
905 antimicrobial against *Clostridioides difficile*. *Sci. Rep.* **10**, 6497 (2020).
- 906 65. Maier, L. *et al.* Unravelling the collateral damage of antibiotics on gut bacteria. *Nature*
907 (2021) doi:10.1038/s41586-021-03986-2.
- 908 66. Kunst, F. *et al.* The complete genome sequence of the gram-positive bacterium *Bacillus*
909 *subtilis*. *Nature* **390**, 249–256 (1997).

- 910 67. Slager, J., Aprianto, R. & Veening, J.-W. Deep genome annotation of the opportunistic
911 human pathogen *Streptococcus pneumoniae* D39. *Nucleic Acids Res.* **46**, 9971–9989
912 (2018).
- 913 68. Baba, T., Bae, T., Schneewind, O., Takeuchi, F. & Hiramatsu, K. Genome Sequence of
914 *Staphylococcus aureus* Strain Newman and Comparative Analysis of Staphylococcal
915 Genomes: Polymorphism and Evolution of Two Major Pathogenicity Islands. *J. Bacteriol.*
916 **190**, 300–310 (2008).
- 917 69. Shiroma, A. et al. First Complete Genome Sequences of *Staphylococcus aureus* subsp.
918 *aureus* Rosenbach 1884 (DSM 20231T), Determined by PacBio Single-Molecule Real-
919 Time Technology. *Genome Announc.* **3**, (2015).
- 920 70. Martin B, García P, Castanié M-P, Claverys J-P. The recA gene of *Streptococcus*
921 *pneumoniae* is part of a competence-induced operon and controls lysogenic induction.
922 *Molecular Microbiology* **15**, 367–379 (1995).
- 923 71. Reed, P. et al. *Staphylococcus aureus* Survives with a Minimal Peptidoglycan Synthesis
924 Machine but Sacrifices Virulence and Antibiotic Resistance. *PLoS Pathog.* **11**, e1004891
925 (2015).
- 926 72. Stamsås, G. A. et al. CozEa and CozEb play overlapping and essential roles in controlling
927 cell division in *Staphylococcus aureus*. *Mol. Microbiol.* **109**, 615–632 (2018).
- 928 73. Huber, P. J. Robust Estimation of a Location Parameter. *Ann. Math. Stat.* **35**, 73–101
929 (1964).
- 930 74. Goldoni, M. & Johansson, C. A mathematical approach to study combined effects of
931 toxicants in vitro: evaluation of the Bliss independence criterion and the Loewe additivity
932 model. *Toxicol. In Vitro* **21**, 759–769 (2007).
- 933 75. R Core Team. R: A language and environment for statistical computing. R Foundation for
934 Statistical Computing, Vienna, Austria. URL <https://www.r-project.org/>. (2021).
- 935 76. RStudio Team. RStudio: Integrated Development Environment for R. RStudio, PBC,
936 Boston, MA URL <http://www.rstudio.com/>. (2021).

- 937 77. Shannon, P. *et al.* Cytoscape: a software environment for integrated models of
938 biomolecular interaction networks. *Genome Res.* **13**, 2498–2504 (2003).
- 939 78. Bajusz, D., Rácz, A. & Héberger, K. Why is Tanimoto index an appropriate choice for
940 fingerprint-based similarity calculations? *J. Cheminform.* **7**, 20 (2015).
- 941 79. Morgan, H. L. The Generation of a Unique Machine Description for Chemical Structures-
942 A Technique Developed at Chemical Abstracts Service. *J. Chem. Doc.* **5**, 107–113
943 (1965).
- 944 80. Milanese, A. *et al.* Microbial abundance, activity and population genomic profiling with
945 mOTUs2. *Nat. Commun.* **10**, 1014 (2019).
- 946 81. Rognes, T., Flouri, T., Nichols, B., Quince, C. & Mahé, F. VSEARCH: a versatile open
947 source tool for metagenomics. *PeerJ* **4**, e2584 (2016).
- 948 82. Edgar, R. C. MUSCLE: multiple sequence alignment with high accuracy and high
949 throughput. *Nucleic Acids Res.* **32**, 1792–1797 (2004).
- 950 83. Guindon, S. *et al.* New algorithms and methods to estimate maximum-likelihood
951 phylogenies: assessing the performance of PhyML 3.0. *Syst. Biol.* **59**, 307–321 (2010).
- 952 84. Kurzawa N, Franken H, Anders S, Huber W, Savitski M. TPP2D: Detection of ligand-
953 protein interactions from 2D thermal profiles (DLPTP). R package version 1.4.1,
954 <http://bioconductor.org/packages/tpp2d>. (2020).
- 955 85. Kurzawa, N. *et al.* Computational analysis of ligand dose range thermal proteome profiles.
956 2020.05.08.083709 (2020) doi:10.1101/2020.05.08.083709.
- 957 86. Kurzawa, N. *et al.* A computational method for detection of ligand-binding proteins from
958 dose range thermal proteome profiles. *Nat. Commun.* **11**, 5783 (2020).
- 959 87. Kanehisa, M. & Goto, S. KEGG: kyoto encyclopedia of genes and genomes. *Nucleic*
960 *Acids Res.* **28**, 27–30 (2000).
- 961 88. Tenenbaum D, M. B. KEGGREST: Client-side REST access to the Kyoto Encyclopedia
962 of Genes and Genomes (KEGG). R package version 1.34.0. (2021).

- 963 89. Geistlinger, L., Csaba, G. & Zimmer, R. Bioconductor's EnrichmentBrowser: seamless
964 navigation through combined results of set- & network-based enrichment analysis. *BMC
965 Bioinformatics* **17**, 45 (2016).
- 966 90. Wu, T. *et al.* clusterProfiler 4.0: A universal enrichment tool for interpreting omics data.
967 *Innovation (N Y)* **2**, 100141 (2021).
- 968 91. Radlinski, L. C. *et al.* Chemical Induction of Aminoglycoside Uptake Overcomes Antibiotic
969 Tolerance and Resistance in *Staphylococcus aureus*. *Cell Chem Biol* **26**, 1355-1364.e4
970 (2019).
- 971 92. Brötz-Oesterhelt, H. & Vorbach, A. Reprogramming of the Caseinolytic Protease by ADEP
972 Antibiotics: Molecular Mechanism, Cellular Consequences, Therapeutic Potential. *Front
973 Mol Biosci* **8**, 690902 (2021).
- 974 93. Weinandy, F. *et al.* A β -lactone-based antivirulence drug ameliorates *Staphylococcus
975 aureus* skin infections in mice. *ChemMedChem* **9**, 710–713 (2014).

976 **Acknowledgements**

977

978 We thank the EMBL Proteomics Core Facility for supporting the 2D-TPP experiments; the
979 Typas lab and in particular Vallo Varik for helpful discussions; Carol Gross, Jan-Willem
980 Veening and Daniel Lopez for strains; Heike Brötz-Oesterhelt for providing the compound
981 ADEP4⁹²; Stephan A. Sieber for providing the compound U1⁹³; Sara Riedel-Christ for her help
982 with *G. mellonella* infection experiments; Zhian Salehian for his support in the construction of
983 the *S. aureus* inducible knockdown mutants. This work was supported by EMBL and the
984 JPIAMR grant COMBINATORIALS to A.T., JPIAMR grant DISRUPT to Mo.K. and A.T. Mi.K.
985 was supported by a fellowship from Swedish Research Council, A.Me. & K.M. by a fellowship
986 from the EMBL Interdisciplinary Postdoc (EI3POD) programme (MSCA COFUND; 664726).

987

988 **Author contributions**

989 E.C. & A.T. conceived and designed the study. O.P.K., Mo.K., G.Z., M.M.S., S.G., W.H. and
990 A.T. supervised the study. E.C. & A.T. designed the experiments: E.C. performed the MIC
991 testing; E.C., K.I. & A.B.-N. performed the two high-throughput screens; E.C. & A.B.-N. did the
992 benchmarking for the screens; E.C. tested all clinical isolates and performed the follow-up
993 work with translation inhibitors in *E. coli*; E.C., Mi.K. & J.S. performed the follow-up work with
994 ticagrelor, except for the TPP experiments which were conducted by A.Ma., E.C. and K. M.,
995 and the CRISPRi knockdown construction, which was carried out by M.T.M.; M.T. and S.G.
996 designed and performed the *G. mellonella* infection experiments. V.K. implemented the screen
997 data analysis pipeline and data visualization interface, with input from W.H. E.C. & V.K
998 analyzed the data from both screens, with input from A.R.B. A.Mi. performed the phylogeny
999 analysis. A.Ma. and E.C. analyzed the TPP data. E.C. designed figures, with inputs from V.K.,
1000 Mi.K., A.Ma., A.T. E.C. and A.T. wrote the manuscript with input from all authors. All authors
1001 approved the final version.

1002

1003 **Competing Interest declaration**

1004 EMBL has filed a patent application on drug combinations identified in this study ("Novel
1005 combinations of antibiotics and non-antibiotic drugs effective in vivo against Gram-positive
1006 bacteria, in particular methicillin-resistant *S. aureus* (MRSA)", European patent application
1007 number EP22207154.0). E.C., S.G. and A.Ty. are listed as inventors.

1008

1009 **Author information**

1010 Correspondence and requests for materials should be addressed to typas@embl.de.

1011

1012 **Figure legends**

1013 **Figure 1. Drug-drug interactions are rare and species-specific in Gram-positive**
1014 **bacteria. a,** Schematic representation of the high-throughput screen. Pairwise combinations
1015 of 65 drugs belonging to several chemical classes and targeting different cellular processes
1016 (**Supplementary Table 1**) were tested at three concentrations in three bacterial species: *S.*
1017 *aureus* (two strains), *B. subtilis* and *S. pneumoniae*. For each strain, 1891 to 2070
1018 combinations were tested in broth microdilution in 384-well-plates, measuring OD_{595nm} over
1019 time. Normalised fitness values were calculated and used to obtain 4 x 4 checkerboards and
1020 assign interactions as synergistic, antagonistic or neutral (Methods, **Extended Data Fig. 1**,
1021 **Supplementary Table 2**). PMF = proton-motive force. **b,** Interaction abundance in each strain
1022 separately, and altogether. Synergy and antagonism frequencies are obtained dividing their
1023 absolute counts by the number of combinations for which the probed fitness space allows to
1024 detect synergy (fitness upon combination ≥ 0.1) or antagonism (fitness upon combination \leq
1025 0.9) discovery (Methods). Total numbers of combinations tested (n) and detected interactions
1026 (i) are shown for each set. **c,** Conservation of interactions among the four strains tested. All
1027 unique interactions detected in the screen (n = 725) are considered to calculate intersection
1028 sets between strains. The total number of interactions in each strain is indicated as set size,
1029 adding up to 945 total interactions in all strains. The 81 interactions (i), involving 47 drugs (d),
1030 are conserved across species (dark red). **d,** Network of conserved interactions between Gram-
1031 positive species. Drugs are grouped according to their targeted cellular process
1032 (**Supplementary Table 1**). Edge thickness is proportional to the number of drug-drug
1033 interactions for each class-class pair. Node size is proportional to the number of drugs in each
1034 class. Only drugs involved in this interaction set are considered (d = 47). Nodes are coloured
1035 according to the targeted cellular processes as in Fig. 1a. **e,** Drug interaction conservation
1036 between species recapitulates phylogeny. Pearson correlation between sequence identity
1037 (based on 40 conserved marker genes) and drug interaction conservation rate between pairs
1038 of species tested here and in a previous study¹.

1039

1040 **Figure 2. Previously uncharacterized synergies in *S. aureus* are active against clinical**
1041 **isolates and in infection models**

1042 **a-b**, Drug interaction networks in *S. aureus*, with drugs grouped according to their class (**a**) or
1043 targeted cellular process (**b**). Unique interactions across both strains tested are considered (i
1044 = 331). Edge thickness represents the proportion of interactions for each node pair,
1045 considering all possible interactions given the number of drugs in each node. Nodes depict
1046 the drug class (**a**) or the targeted cellular process (**b**), and size is proportional to the number
1047 of drugs in the represented class/process. Only interacting drugs are considered ($d = 62$).
1048 Synergies, antagonisms and nodes are coloured according to Fig. 1. **c**, Novel and previously
1049 reported interactions detected in *S. aureus*. Interactions are considered known if reported in
1050 any *S. aureus* strain (**Supplementary Table 4**). **d-e**, Novel synergies are effective against
1051 MRSA clinical isolates *in vitro* (**d**) and *in vivo* in the *G. mellonella* infection model (**e**).
1052 Teicoplanin (TEC) synergies with cefepime (FEP) and trimethoprim (TMP) were validated
1053 against a tigecycline-resistant MRSA clinical isolate (**Supplementary Table 1**) in 8 x 8 broth
1054 microdilution checkerboards (**d**) and in *G. mellonella* infection model (**e**). For checkerboards
1055 the median fitness (OD_{595nm} at 7.5h normalised by no-drug controls) across two biological
1056 replicates is shown (**Extended Data Fig. 7, Supplementary File**). For *G. mellonella*
1057 experiments, larvae were infected with the same MRSA isolate and treated with single drugs
1058 or combinations. The percentage of surviving larvae after treatment and in the untreated
1059 controls was monitored over time. Uninfected and untreated (vehicle only) controls are shown.
1060 Drugs were tested in combination at the same concentration indicated for each drug. Data
1061 points represent the mean and error bars indicate standard error ($n = 10$ for each condition,
1062 three independent experiments).

1063

1064 **Figure 3. Distinct synergies between drugs targeting the same cellular process across**
1065 **Gram-positive and -negative species. a**, Drugs targeting the same biological process often
1066 interact synergistically, whereas antagonisms are prevalent between drugs targeting different

1067 processes (*S. aureus*: $p = 9.9\text{e-}07$, χ^2 test; *S. pneumoniae*: $p = 4.7\text{e-}08$, χ^2 test). Non-antibiotic
1068 drugs ($n = 8$) are excluded from this analysis, as their targeted processes are heterogeneous
1069 or unknown. **b**, Gram-positive species exhibit frequent synergistic interactions between
1070 protein-synthesis inhibitors, whereas cell-wall biosynthesis inhibitors predominantly synergize
1071 in Gram-negative species. Prevalence of interactions between protein-synthesis inhibitors and
1072 between cell-wall biosynthesis inhibitors in Gram-negative and Gram-positive species (for
1073 protein synthesis inhibitors: $p=1.8\text{e-}08$; for cell-wall biosynthesis inhibitors: $p=0.0038$, χ^2 test).
1074 **c**, Protein-synthesis inhibitors can also synergize in Gram-negative species when the drug
1075 permeability bottleneck is abolished. Synergistic combinations in Gram-positive species were
1076 tested in 8×8 broth microdilution checkerboards in wild-type *E. coli* and in the OM-defective
1077 *E.coli lptD4213* strain³⁷. Interaction score distributions for each combination are significantly
1078 different between the two strains. Interactions were assigned with the same criteria used in
1079 the screen, with synergies corresponding to distributions with first quartile < -0.1 . The first
1080 quartile value is shown in all cases. CLR, clarithromycin; CLI, clindamycin; AZM, azithromycin;
1081 LZD, linezolid; CHL, chloramphenicol (CLR + CLI: $p = 2.2\text{e-}16$; CLR + AZM: $p = 5.3\text{e-}13$; CLR
1082 + CHL: $p = 2.2\text{e-}16$; CLR + LZD: $p = 4.4\text{e-}08$, Wilcoxon test). **d**, Differences in beta-lactam
1083 synergy prevalence between Gram-negative and Gram-positive species are related to
1084 differences in drug target redundancy, that is the Penicillin Binding Proteins (PBPs) they
1085 encode in their genomes. Pearson correlation between number of PBPs (**Supplementary**
1086 **Table 5**) and the frequency of synergies between beta-lactams for each strain tested.
1087

1088 **Figure 4. Prevalent interactions between non-antibiotic drugs and antibiotics in *S.***
1089 ***aureus*.** **a**, Interactions of non-antibiotic drugs between themselves and with antibiotics are as
1090 common as interactions between two antibiotics. This motivated us to expand the non-
1091 antibiotic panel tested. Synergy and antagonism frequencies are calculated as in Fig. 1b. **b**,
1092 Interactions between non-antibiotics and antibiotics in the extended non-antibiotic screen in *S.*
1093 *aureus* DSM 20231. 44 additional non-antibiotic drugs were screened in combination with 62
1094 drugs belonging to the original drug panel, using the same experimental setup and the same

1095 data analysis pipeline, in *S. aureus* DSM 20231 (Methods). Synergy and antagonism
1096 frequencies are calculated as in Figure 1b. **c**, Non-antibiotics with antibacterial activity, for
1097 which the MIC was among tested concentrations ($n = 13$), engage in more interactions than
1098 non-antibiotics for which an MIC does not exist or was not within the tested concentration range
1099 ($n = 31$). **d**, All interactions between non-antibiotic and antibiotics detected in *S. aureus* DSM
1100 20231 in the original ($i = 87$) and in the extended ($i = 197$) non-antibiotic screen. **e-f**, The
1101 nonsteroidal anti-inflammatory ibuprofen synergizes with gentamicin in MRSA clinical isolates
1102 *in vitro* (**e**) and in *in vivo* infection models (**f**). Gentamicin synergizes with ibuprofen and
1103 ticagrelor in an MRSA-clinical isolate with additional resistance to linezolid (**Supplementary**
1104 **Table 1**) in 8 x 8 broth microdilution checkerboards (**e**) and in *G. mellonella* infection model (**f**).
1105 Controls and results are obtained and represented as in Fig. 2d-e. GEN, gentamicin; IBU,
1106 ibuprofen.

1107

1108 **Figure 5. The antiplatelet ticagrelor affects *S. aureus* metabolism and synergizes with**
1109 **cationic antibiotics by altering *S. aureus* surface charge. a-b**, Volcano plots highlighting
1110 abundance or stability hits in whole-cell (**a**) and lysate 2D-TPP data (**b**). The x-axis represents
1111 the effect size of protein abundance or stability change⁸⁶ (Methods), and the y-axis
1112 corresponds to the statistical significance ($\log_2(F\text{-statistic})$). For visualisation purposes, when
1113 the F-statistic was 0, it was transformed to 1. **c-e**, Ticagrelor synergizes with gentamicin *in vitro*
1114 at growth inhibition (**c**, **Extended Data Fig. 11a, Supplementary File**) and killing level (**d**,
1115 mean across four biological replicates; error bars represent standard error, drugs tested in
1116 combination at same concentration indicated for each drug), and *in vivo* (**e**) against an MRSA
1117 isolate resistant to tigecycline (**Supplemental Table 1**). Results for **c** and **e** are obtained and
1118 represented as described in Fig. 2d-e. GEN, gentamicin; TIC, ticagrelor. **f**, Growth (endpoint
1119 OD_{595nm}, corresponding to the beginning of stationary phase for the control strain MM76,
1120 Methods, **Supplementary File**) measured in the presence of serial two-fold dilutions of
1121 gentamicin, normalised by no-drug controls, in the *S. aureus* IPTG-inducible knockdown
1122 mutants *dltABCD* and *tagG* and their control strain MM76 (Methods, **Supplementary Table**

1123 1), in presence or absence of 500 μM IPTG to induce maximal knockdown of the gene targeted
1124 (median across four biological replicates; error bars represent standard error). All strains are
1125 grown in presence of 5 $\mu\text{g/ml}$ erythromycin and 10 $\mu\text{g/ml}$ chloramphenicol to maintain the
1126 CRISPRi plasmids⁷² (Methods). For all controls and full growth curves see Supplementary File.
1127 g, *S. aureus* Newman surface charge changes upon exposure to ticagrelor. The fraction of
1128 positively charged unbound cytochrome C is measured after incubation of drug treated and
1129 untreated samples ($n = 6$, mean and standard error are shown, Methods). For all controls and
1130 cytochrome c standard curve see **Extended Data Fig. 12g**.

1131

1132 **Extended data figure legends**

1133 **Extended Data Fig. 1. Data analysis pipeline.** Raw growth curves based on measurement
1134 of OD_{595nm} over 14h were processed as depicted. Background was removed by subtracting
1135 the OD_{595nm} at the first time point (when this was not affected by artefacts) from all the following
1136 measurements (Methods). All curves within a plate were trimmed beyond the point that the
1137 no-drug controls within the plate (6 wells) entered stationary phase. The OD_{595nm} measurement
1138 at this time-point was then normalised per plate by the robust mean of the no-drug control
1139 wells (6 per plate), resulting in fitness values (Methods) that were used to obtain 4 x 4
1140 checkerboards for each combination. Bliss (ε) scores were then calculated as follows: $\varepsilon = f_{d1,d2}$
1141 – $f_{d1} * f_{d2}$, where $f_{d1,d2}$ corresponds to the observed fitness in the presence of the drug
1142 combination, and f_{d1} and f_{d2} correspond to the fitness in the presence of each single drug.
1143 Single-drug fitness values were estimated from drug-combination fitness by minimizing the
1144 sum of residuals squared of the Bliss independence model (Methods, [eq. 2]). Interactions
1145 fulfil two criteria: (i) FDR < 0.05, after applying a resampling procedure with 10,000 repetitions
1146 of a two-sided Wilcoxon rank-sum test, to compare the ε distribution of each combination
1147 tested to the overall ε distribution; and (ii) a quartile-based effect size threshold examining the
1148 ε distribution of each combination, with synergies assigned if first quartile (green line) < -0.1
1149 and antagonisms if third quartile > 0.1 (yellow line).

1150

1151 **Extended Data Fig. 2. Quality control of the main interaction screen and assessment of**
1152 **fitness calculation methods.** **a-b**, Donor (**a**) and recipient (**b**) drug fitness correlation
1153 between biological replicates. Pearson correlation is calculated between biological replicates,
1154 corresponding to different experimental runs/batches. **c**, Technical replicate correlation.
1155 Pearson correlation is calculated between replicate wells within the same plate for combination
1156 plates (where donor drugs were added) and control recipient plates (where no donor drug was
1157 added), for the four strains screened. Plates for which technical plate correlation was < 0.7
1158 (red) were removed from the data. **d**, Endpoint-OD- and AUC-based fitness values for all
1159 strains are highly correlated (Pearson correlation, $R = 0.95$, $p < 2.2e-16$, $n = 223055$). **e**,
1160 Performance of endpoint OD- and AUC-based measurements in terms of precision-recall
1161 against the benchmarking set. Precision-recall curves are shown for q-value intervals
1162 increasing by 0.01. Curves highlighted correspond to the effect-size cutoff selected for the
1163 screen (interaction score = $|0.1|$). The selected significance cutoff (FDR < 0.05) is marked. **f-**
1164 **g**, Comparison between estimated and experimentally measured single-drug fitness for donor
1165 (**f**) (Pearson correlation, $R = 0.96$, $p < 2.2e-16$, $n = 5208$) and recipient (**g**) drugs (Pearson
1166 correlation, $R = 0.98$, $p < 2.2e-16$, $n = 1718$).

1167

1168 **Extended Data Fig. 3. Screen benchmarking.** **a**, 161 drug combinations were selected for
1169 benchmarking, including hits and neutral interactions, and tested in extended concentration
1170 checkerboards (8 x 8). Fitness values and interaction scores were calculated as in the high-
1171 throughput screen (Methods). **b**, Combinations were selected to equally represent the four
1172 strains tested. **c**, Screen precision and recall against the benchmarking set are assessed for
1173 different effect-size thresholds. Precision-recall curves are shown for FDR intervals ranging
1174 from 0 to 1, increasing by 0.005. The chosen significance value for the screen (FDR < 0.05)
1175 is highlighted for the effect-size curve ($|0.1|$) providing best precision and recall. The addition
1176 of weak interactions (effect-size threshold $|0.08|$, Methods) increases slightly the recall.
1177 $|efsize|$ =effect size. **d**, True-positive (TP), true-negative (TN), false-positive (FP) and false-

1178 negative (FN) abundance in the benchmarking set for optimal thresholds. As for most screens,
1179 conservative cutoffs for interactions minimize FPs with a cost on the number of FNs.

1180

1181 **Extended Data Fig. 4. Interaction conservation within Gram-positive species and across**
1182 **the Gram-positive/-negative divide.** **a**, There is no significant difference between synergy
1183 and antagonism prevalence among conserved and non-conserved interactions, regardless of
1184 whether non-antibiotic drugs, whose targets are multiple or unknown, are considered ($p =$
1185 0.592, χ^2 test) or not ($p = 0.327$, χ^2 test). Only interactions conserved across at least two
1186 species are considered ($n = 81$, **Fig. 1c**). **b**, Drugs targeting more conserved cellular
1187 processes tend to have more conserved interactions. Interaction conservation ratio for each
1188 drug class across species is calculated as the ratio between conserved and non-conserved
1189 interactions. **c**, Synergy and antagonism abundance of unique interactions shared by at least
1190 one Gram-negative and Gram-positive strain – edges are colour-coded according to whether
1191 interaction is synergistic (green) or antagonistic (yellow). **d**, Conserved interactions across at
1192 least one Gram-negative and Gram-positive strain. EC, *E.coli*; PA, *P. aeruginosa*; ST, *S.*
1193 *Typhimurium*; SA, *S. aureus*; SP, *S. pneumoniae*; BS, *B. subtilis*. **e**, Heatmap of conserved
1194 interactions across Gram-positive and Gram-negative bacteria. Interactions that are also
1195 conserved across multiple Gram-positive species are highlighted.

1196

1197 **Extended Data Fig. 5. Interaction networks with drugs grouped according to their class**
1198 **or their targeted cellular processes for *B. subtilis* (a, c) and *S. pneumoniae* (b, d).** Node
1199 size and colour and edge thickness are depicted as in Fig. 2a-b. i, number of interactions; d,
1200 drugs involved in the interactions (may differ from number of drugs tested in screen).

1201

1202 **Extended Data Fig. 6. Drug interaction fingerprint recapitulates their functional and**
1203 **chemical classes.** **a**, Drugs clustered according to their interactions with all other drugs in
1204 main screen. For each drug, quartile-based Bliss interaction scores (Methods) with all the
1205 other drugs ($n = 65$) in all four strains (x-axis) are considered; drug interaction fingerprints are

1206 then clustered according to their cosine similarity. All interaction cumulative scores are
1207 considered, regardless of their significance. Clusters enriched in drugs belonging to the same
1208 classes, targeting the same processes, and/or chemically similar, are highlighted. Negative,
1209 positive and neutral Bliss scores are depicted in shades of green, yellow, and in white,
1210 respectively. Combinations that were not tested in a given strain are in grey. **b**, Drug clustering
1211 according to their chemical structure similarity (Methods). In both panels, drugs are coloured
1212 according to their targeted cellular process (colour code as in Fig. 1).

1213

1214 **Extended Data Fig. 7. Antibiotic synergies detected in screen are effective against**
1215 **MRSA clinical isolates.** Teicoplanin synergies with cefepime (**a**) and trimethoprim (**b**) were
1216 tested in 8 x 8 checkerboards in model MSSA (Newman and DSM 20231) and MRSA
1217 (USA300) strains, and in 5 clinical MRSA strains from different worldwide-prevalent clonal
1218 complexes, isolated from different infection sites, and bearing different multidrug resistance
1219 profiles (**Supplementary Table 1**). Results are obtained and represented as in Fig. 2d. One
1220 representative checkerboard of n = 2 (biological replicates) is shown here (for the second
1221 replicate see Supplementary File). Lzd-R, linezolid-resistant; Tig-R, tigecycline-resistant.

1222

1223 **Extended Data Fig. 8. Interactions between drug functional classes in Gram-positive**
1224 **and Gram-negative species.** **a**, Interactions between all drug classes (based on cellular
1225 target) in Gram-positive (**a**) and Gram-negative (**b**) species. The absolute count for each class-
1226 class interaction is indicated. PMF = proton-motive force. Interactions between drugs tested in
1227 all strains are considered. Interactions conserved across different strains are considered as
1228 distinct occurrences. **c-f**, Heatmaps of interactions between protein synthesis inhibitors (**c-d**)
1229 and between cell-wall biosynthesis inhibitors (**e-f**). Bliss interaction scores are averaged across
1230 strains if the same interaction is found in more than one strain. In rare cases in which opposite
1231 interactions are found in two different strains (n = 4, **c**; n = 2, **d**; n = 2, **e**; n = 8, **f**), the strongest
1232 one is shown here.

1233

1234 **Extended Data Fig. 9. Protein synthesis inhibitors interact neutrally in wild-type *E. coli***
1235 **BW25113 and synergistically in *E. coli* *IptD*4213 mutant.** Checkerboards from which Bliss
1236 interaction scores shown in **Fig. 3c** were derived. Combinations were tested in each strain in
1237 two biological and two technical replicates. Synergy, green; Neutrality, grey.

1238

1239 **Extended Data Fig. 10. Non-antibiotic drug screen and benchmarking.** **a**, Schematic
1240 representation of non-antibiotic drug high-throughput screen. 44 drugs belonging to different
1241 therapeutic classes (**Supplementary Table 6**) were tested in combination with 62 antibiotics
1242 at three concentrations in *S. aureus* DSM 20231. The resulting 2728 combinations were tested
1243 in broth microdilution (Methods). **b**, 37 drug combinations (**Supplementary Table 6**) were
1244 selected for benchmarking and tested in 8 x 8 concentration checkerboards (Methods). **c**,
1245 True-positive (TP), true-negative (TN), false-positive (FP) and false-negative (FN) abundance
1246 in the benchmarking set for optimal thresholds shown in **d**. **d**, Screen precision and recall
1247 against the benchmarking set are assessed for different effect-size thresholds. Precision-recall
1248 curves are shown for FDR intervals ranging from 0 to 1, increasing by 0.005. The chosen
1249 significance value for the screen (FDR < 0.05) is highlighted for the effect-size curve ($|0.1|$)
1250 providing best precision and recall. **e-f**, Interaction abundance for classes of non-antibiotics (**e**)
1251 and classes of antibiotics (**f**). Interactions detected in *S. aureus* DSM 20231 between
1252 antibiotics classes and 52 non-antibiotics tested in both the original screen ($n = 8$) and the
1253 extended screen ($n = 44$) were considered ($n = 245$). PMF, Proton-motive force; CCB, calcium-
1254 channel blocker; PPI, proton-pump inhibitors; ARB, angiotensin-receptor blocker. Synergies
1255 are depicted in green, antagonisms in yellow.

1256

1257 **Extended Data Fig. 11. Synergies between antibiotics and non-antibiotic drugs detected**
1258 **in model *S. aureus* strains are also effective in MRSA clinical isolates.** Gentamicin
1259 synergies with ibuprofen (**a**) and ticagrelor (**b**) were tested in 8 x 8 checkerboards in model
1260 MSSA (Newman and DSM 20231) and MRSA (USA300) strains, and in 5 clinical MRSA strains
1261 from different clonal complexes, isolated from different infection sites, and bearing different

1262 resistance profiles (**Supplementary Table 1**). Results are obtained and represented as in Fig.
1263 2d. One representative checkerboard of n = 2 (biological replicates) is shown here (for the
1264 second replicate see Supplementary File). Lzd-R, linezolid-resistant; Tig-R, tigecycline-
1265 resistant.

1266

1267 **Extended Data Fig. 12. Ticagrelor affects purine and teichoic acid biosynthesis.** **a**, KEGG
1268 enrichment of hits at 5% FDR from whole-cell or lysate samples. Only sets yielding significant
1269 enrichments (whole-cell down- and up-regulation, and lysate stabilisation) are shown
1270 (**Supplementary Table 7**). The first 15 terms in order of significance are shown. The dashed
1271 lines mark the enrichment significance cut-off (adjusted p-value < 0.05, Fisher's exact test).
1272 The number of protein hits is annotated for each term. **b**, Thermal stability profiles of members
1273 of the purine biosynthesis pathway. Protein fold change is shown for each temperature and
1274 ticagrelor concentration. **c**, Growth (endpoint-OD_{595nm} after 11h, corresponding to the
1275 beginning of stationary phase for the untreated control, Methods) measured in the presence
1276 of serial two-fold dilutions of ticagrelor in presence or absence of purines at the indicated
1277 concentration, normalised by no-drug controls, in *S. aureus* Newman in SSM9PR defined
1278 medium (median across four biological replicates; error bars represent standard error;
1279 Methods). **d**, Ticagrelor synergizes with nisin *in vitro*. Results are obtained and represented as
1280 in Fig. 2d. **e**, Thermal stability profiles of proteins involved in teichoic acid biosynthesis,
1281 represented as in **b**. **f**, Growth (endpoint OD_{595nm}, corresponding to the beginning of stationary
1282 phase for the control strain MM76, Methods, **Supplementary File**) measured in the presence
1283 of serial two-fold dilutions of nisin, normalised by no-drug controls, in the *S. aureus* IPTG-
1284 inducible knockdown mutants *dltABCD* and *tagG* and their control strain MM76 (Methods), in
1285 presence or absence of 500 µM IPTG to induce maximal knockdown of the gene targeted
1286 (median across four biological replicates; error bars represent standard error). All strains are
1287 grown in presence of 5 µg/ml erythromycin and 10 µg/ml chloramphenicol to maintain the
1288 CRISPRi plasmids⁷² (Methods). For all controls and full growth curves see Supplementary File.
1289 **g**, Raw data (OD_{410nm}) from Fig. 5g are shown alongside all controls (samples not incubated

1290 with 250 µg/ml cytochrome c, cytochrome c standard curve including buffer control). The linear
1291 fit for the cytochrome c standard curve used to infer the unbound cytochrome C fraction in
1292 supernatants is shown ($n = 4$, mean and standard error of the mean are shown. Data points
1293 represent reads ($n=4$ biological replicates for each condition, Methods).

1294

1295 **Supplementary File**

1296 This file contains the second biological replicates for checkerboards in **ED Fig. 7a-b** and **ED Fig.**
1297 **11a-b** and full growth curves and controls for data in **Fig. 5f** and **Extended Data Fig. 12c** and f.

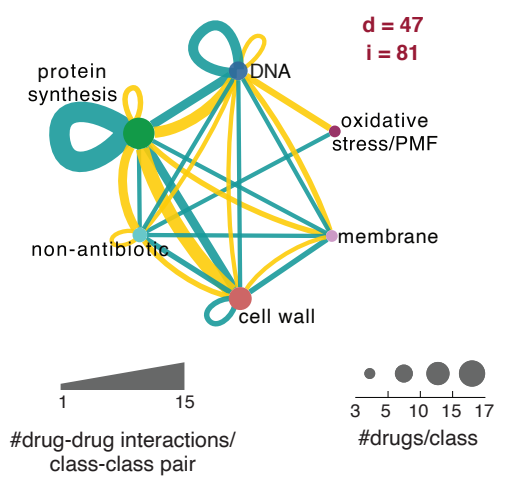
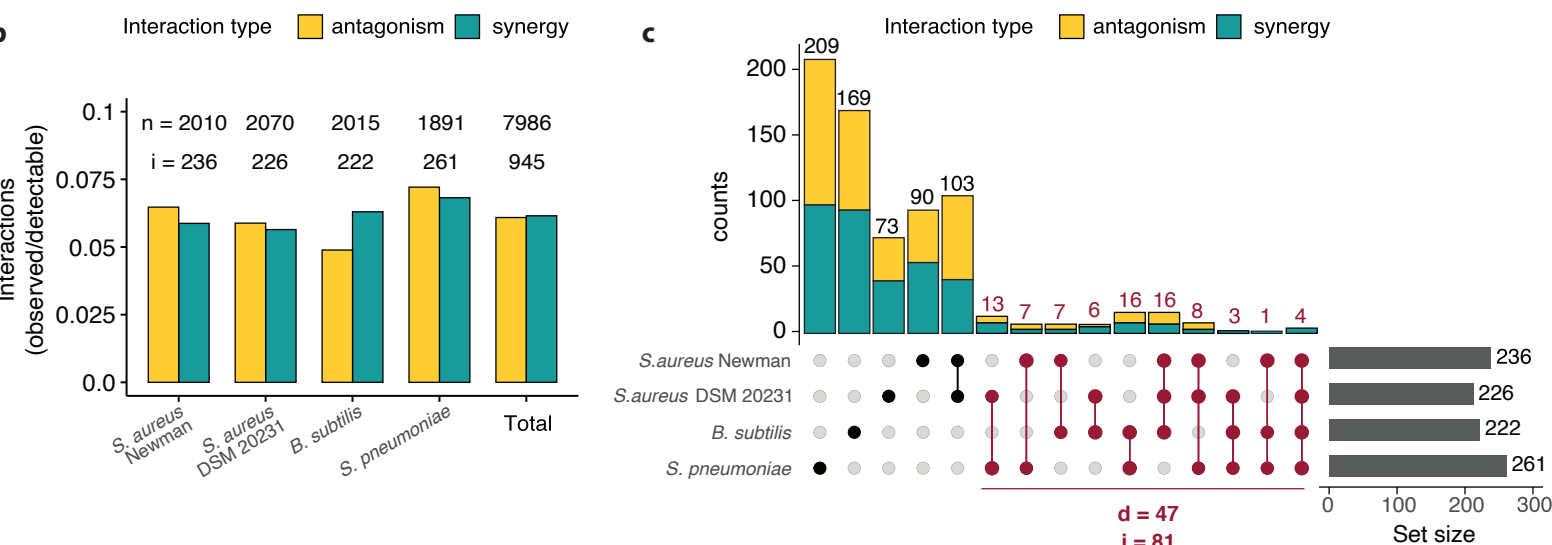
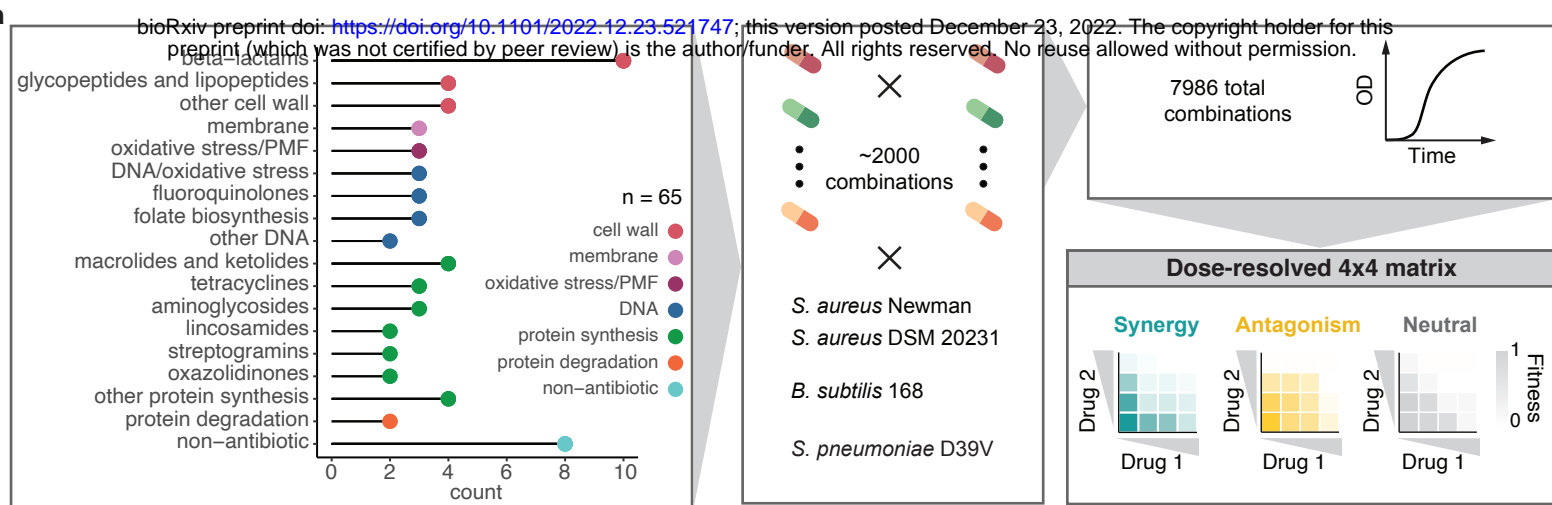


Figure 1

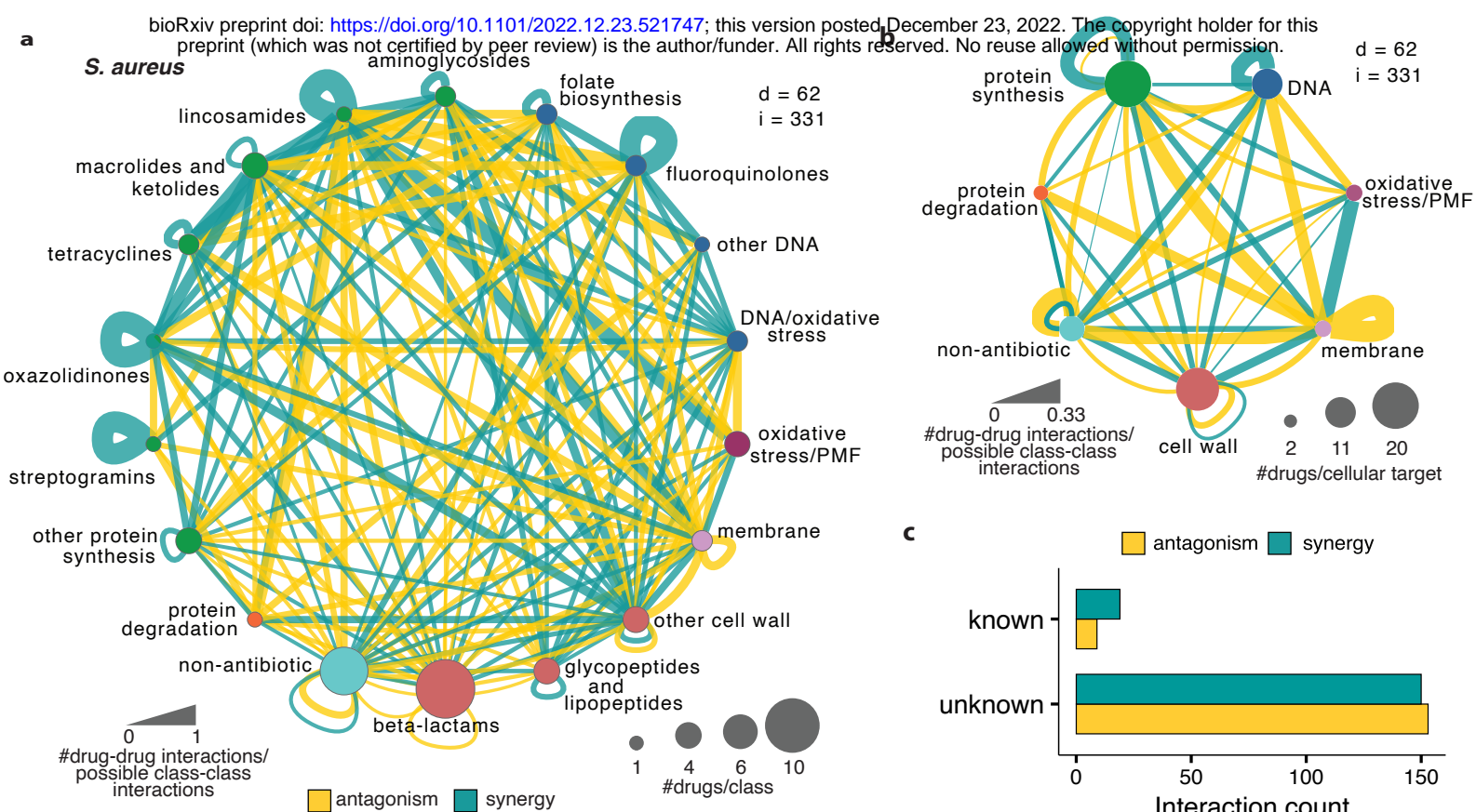


Figure 2

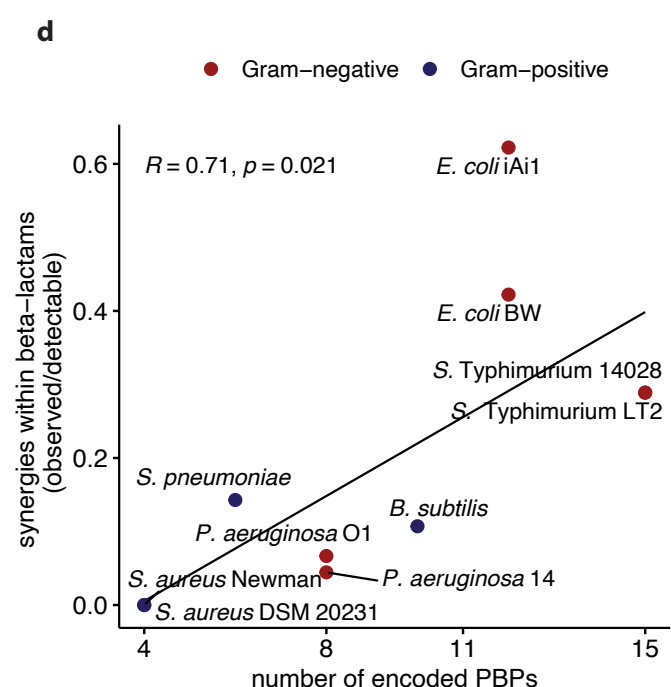
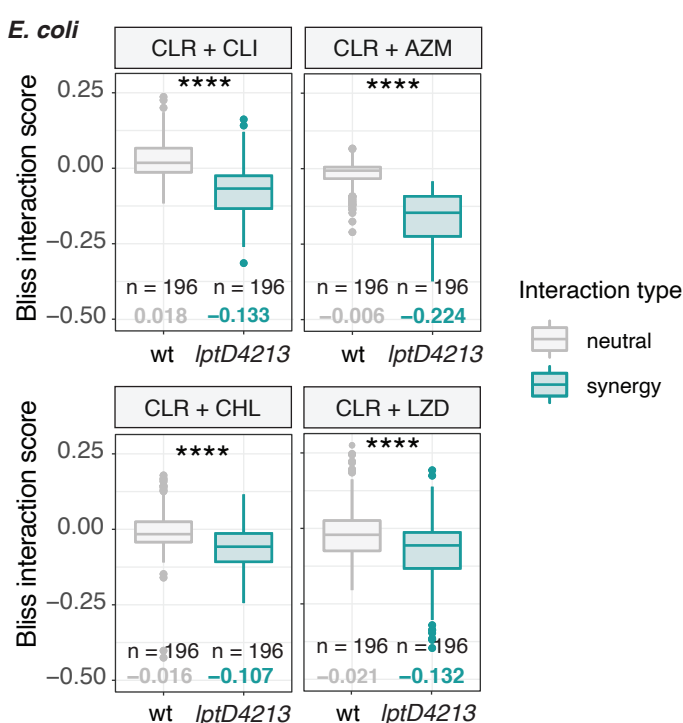
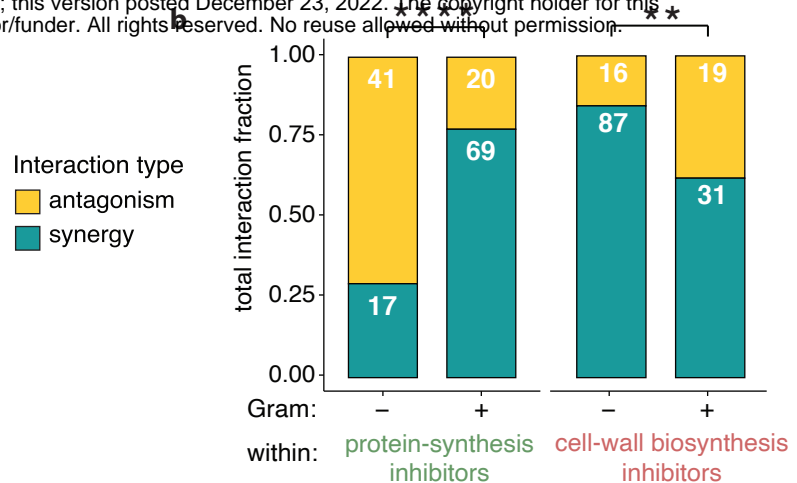
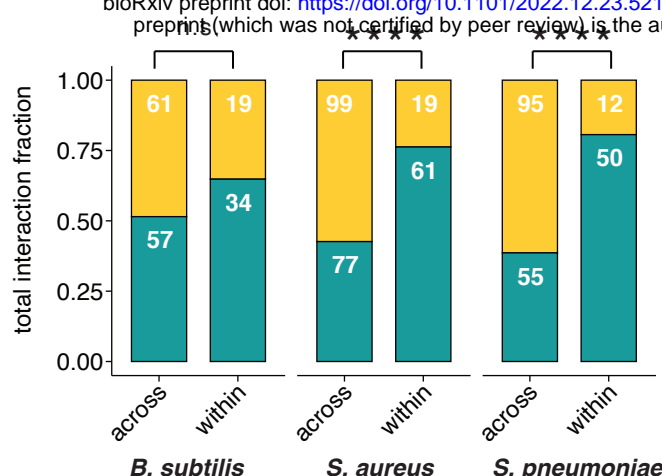
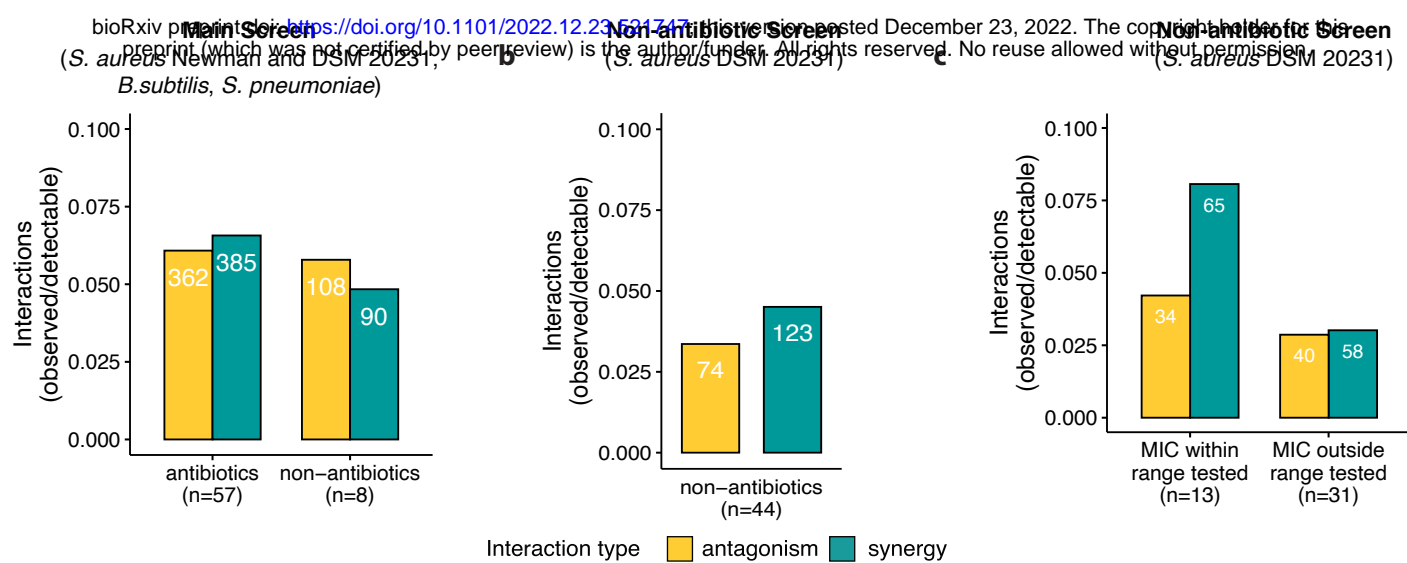
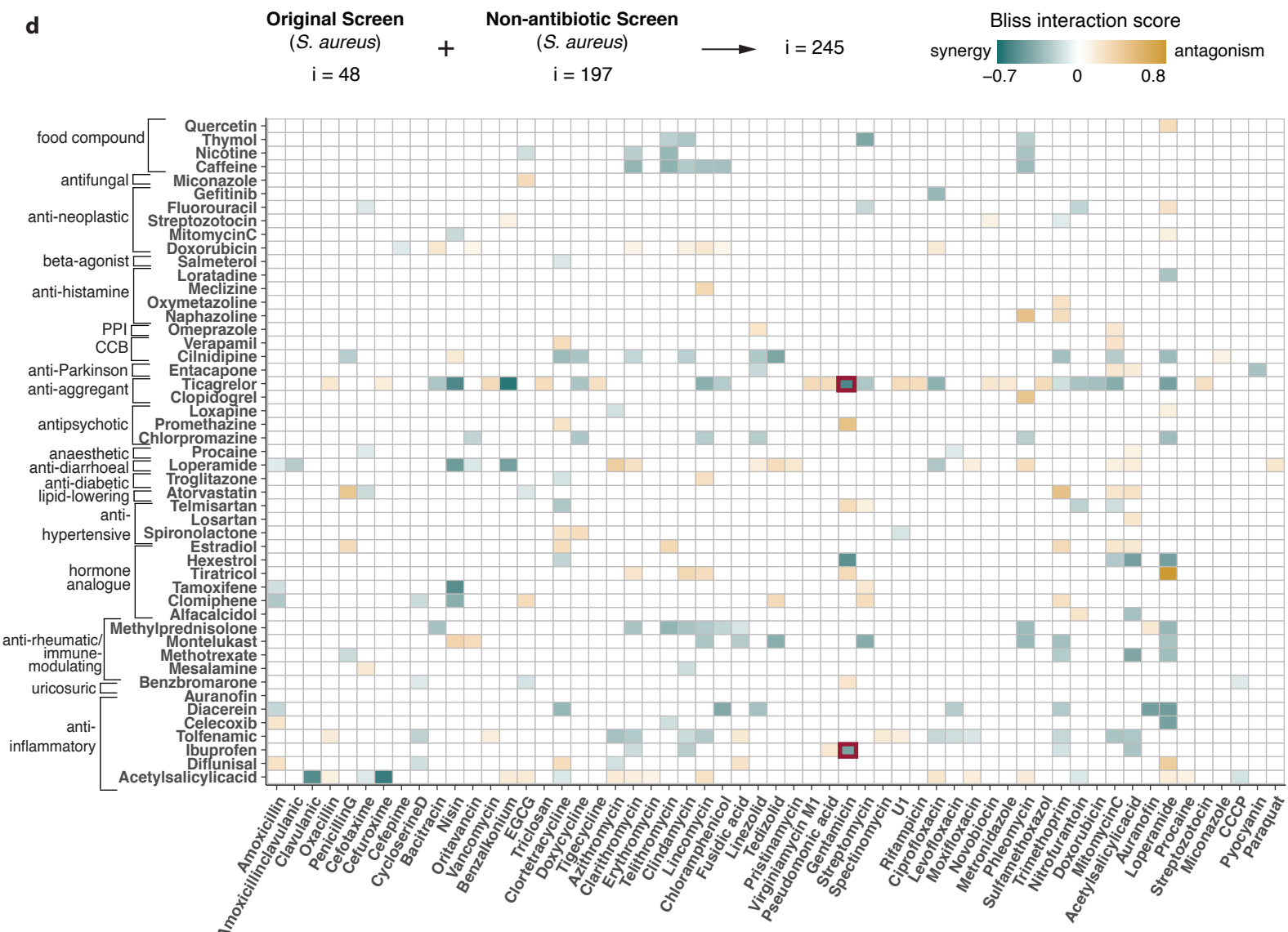


Figure 3

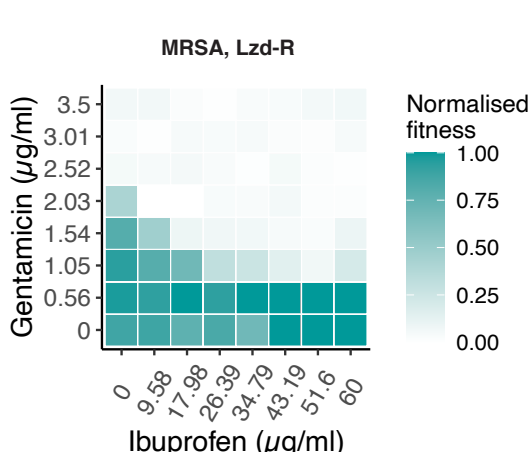
a



d



e



f

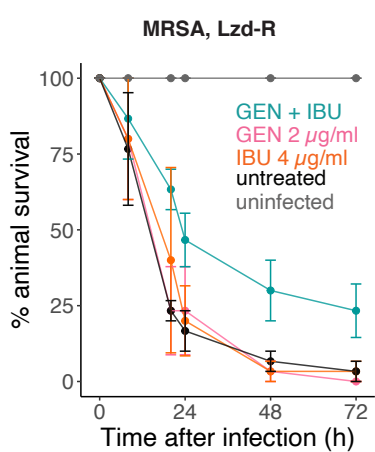


Figure 4

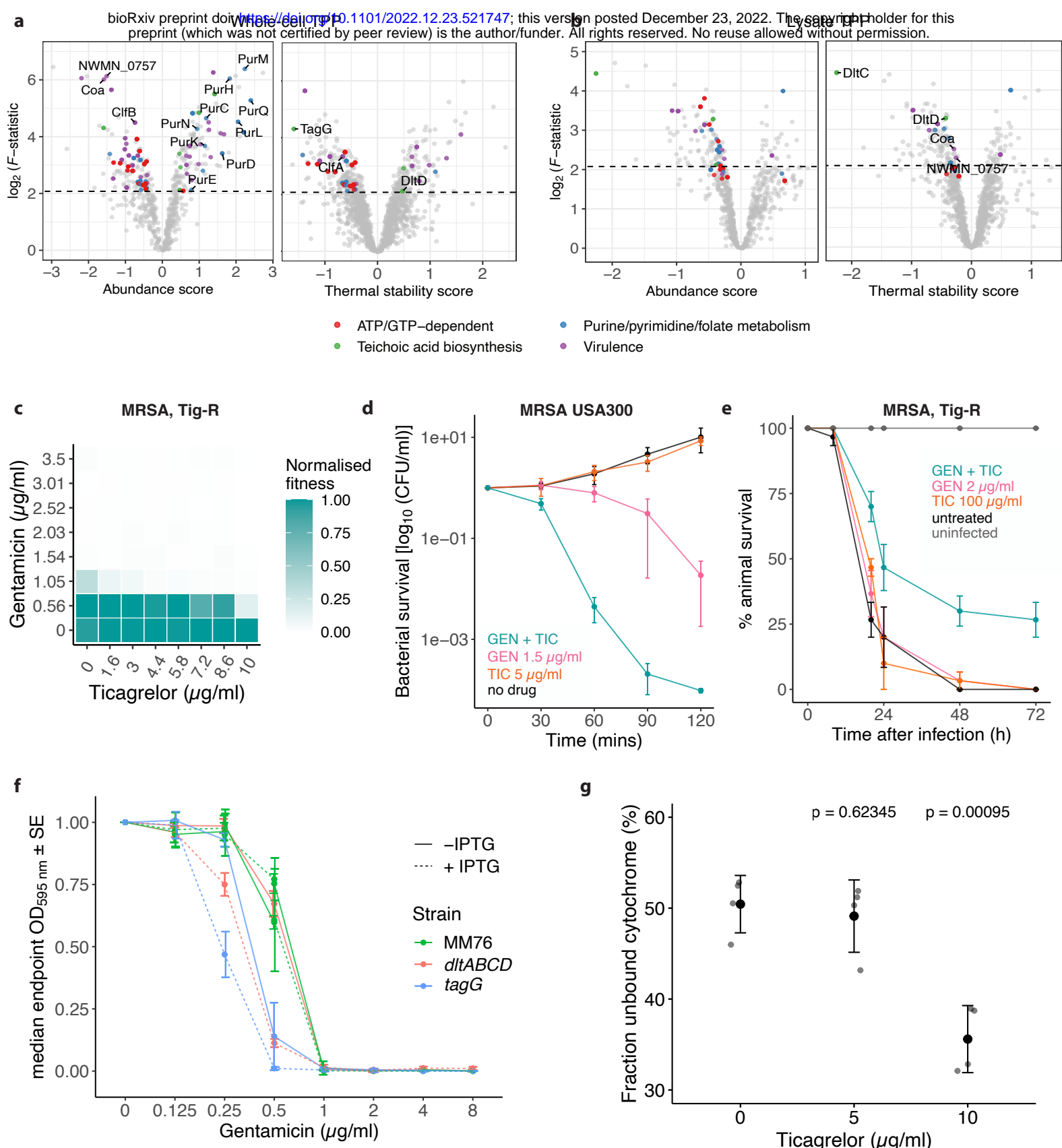
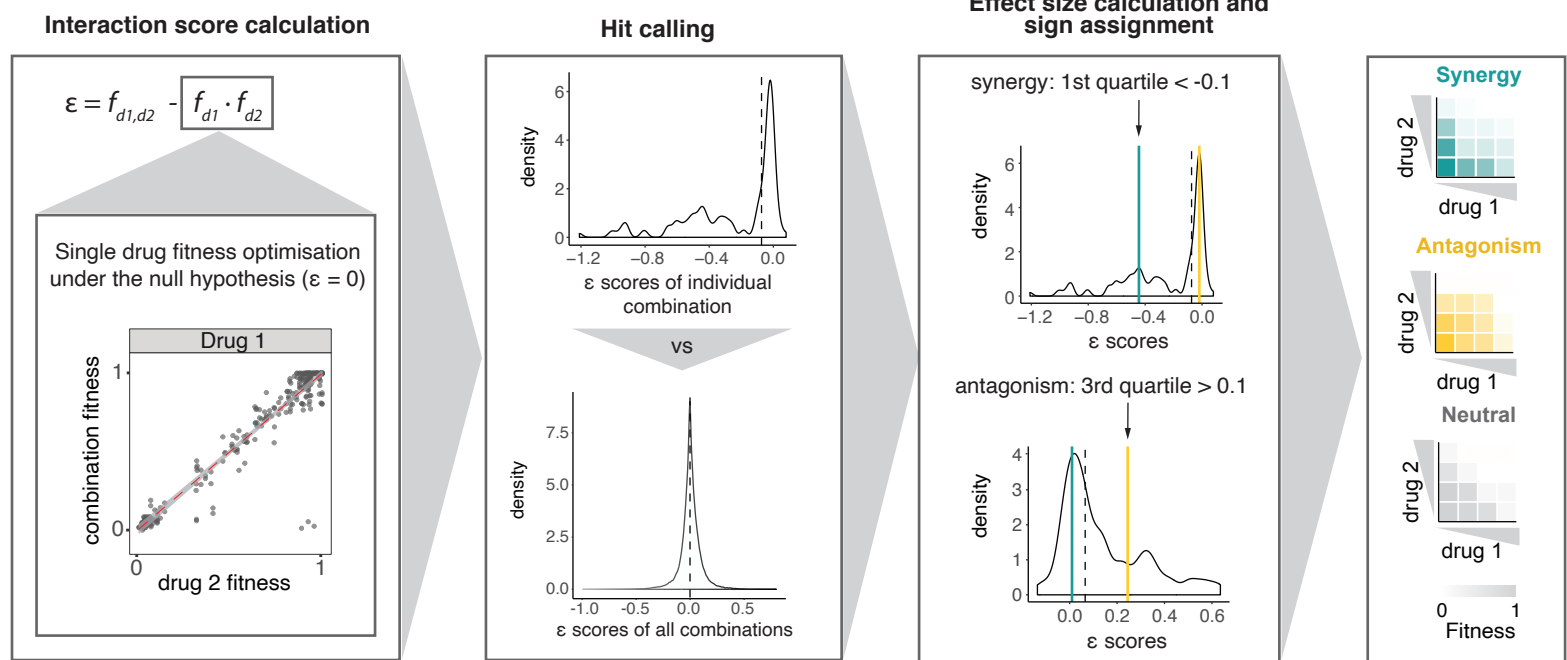
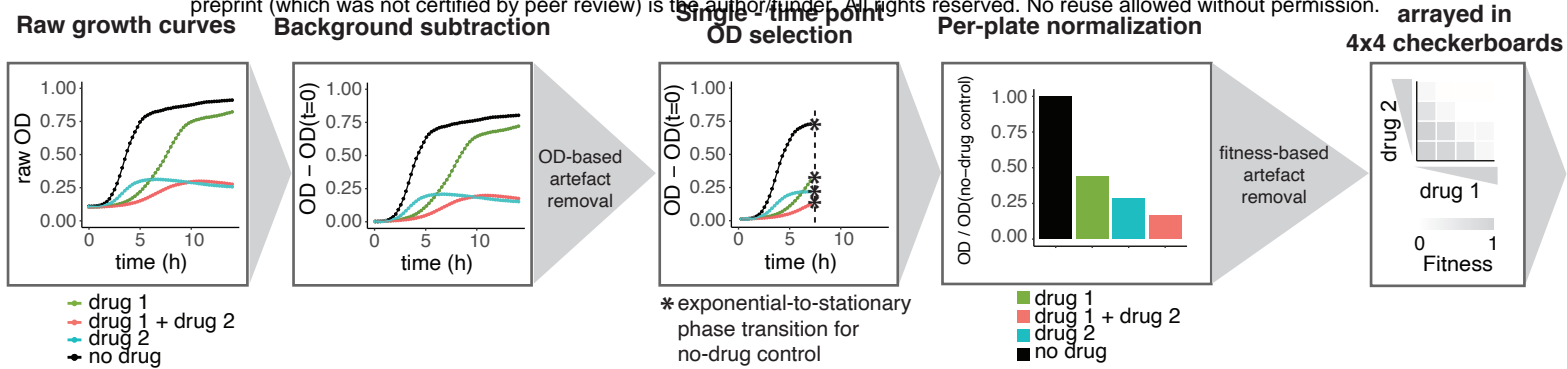
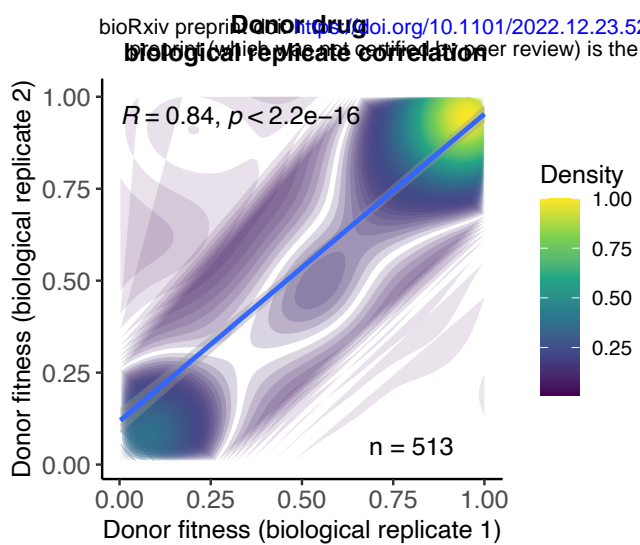


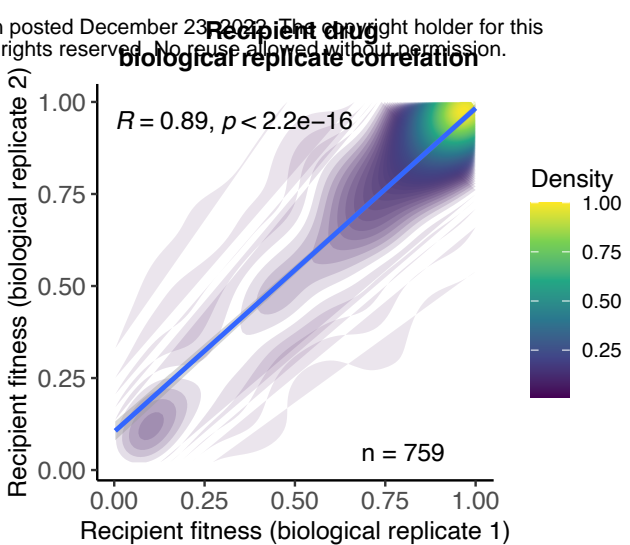
Figure 5



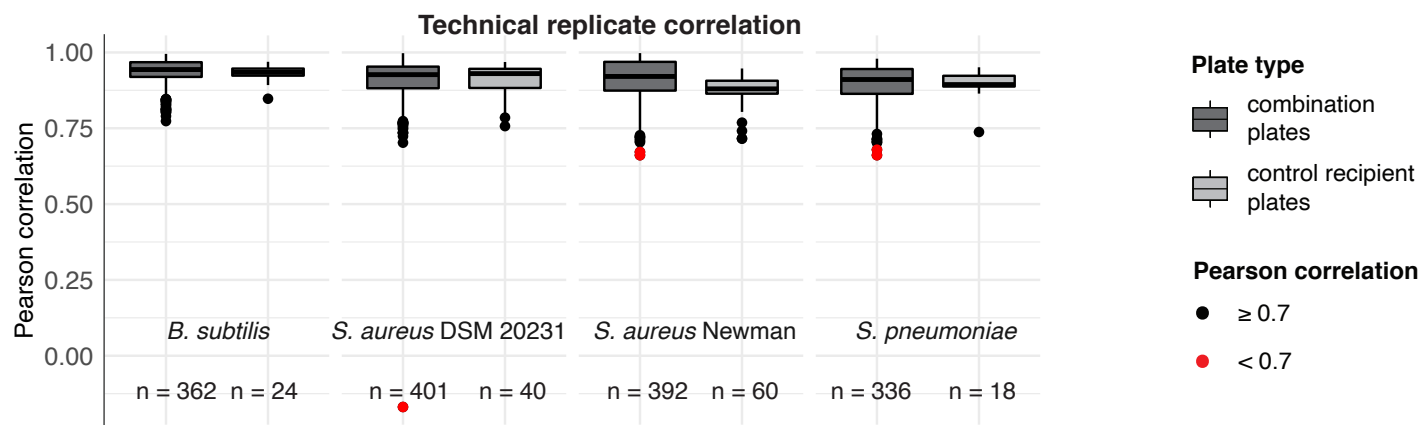
a



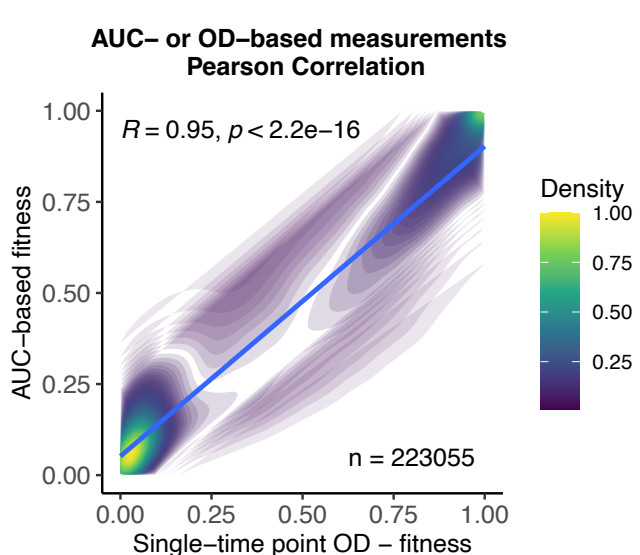
b



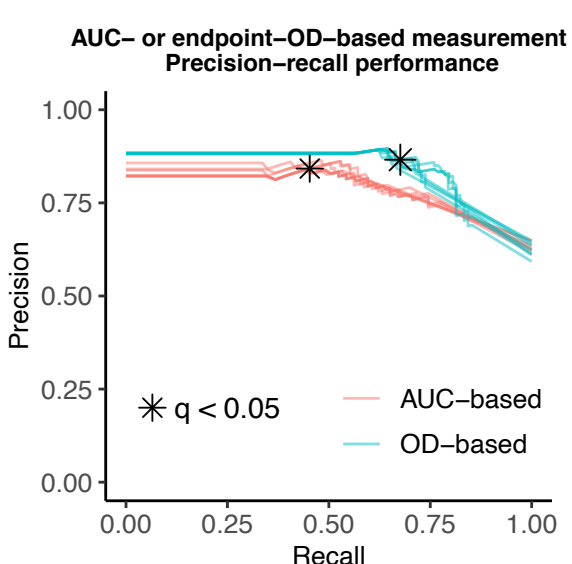
c



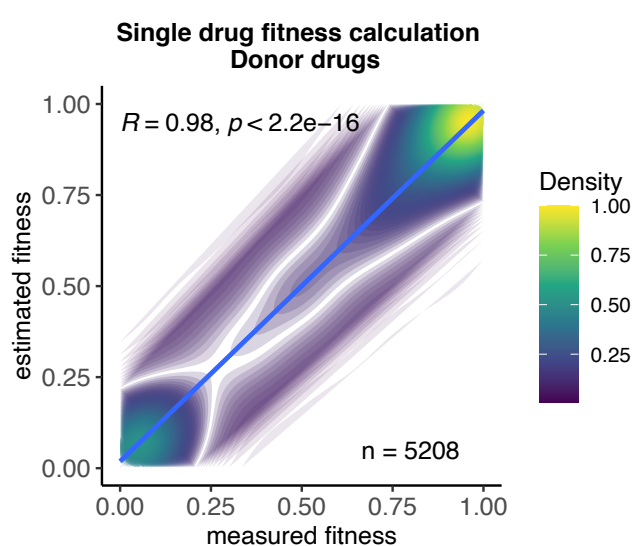
d



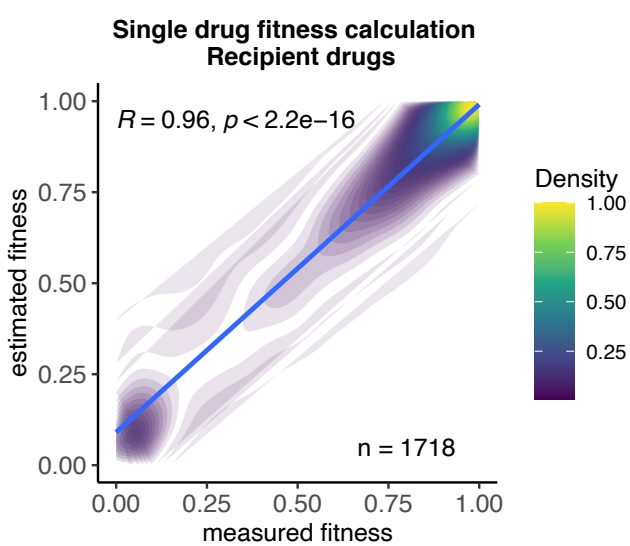
e



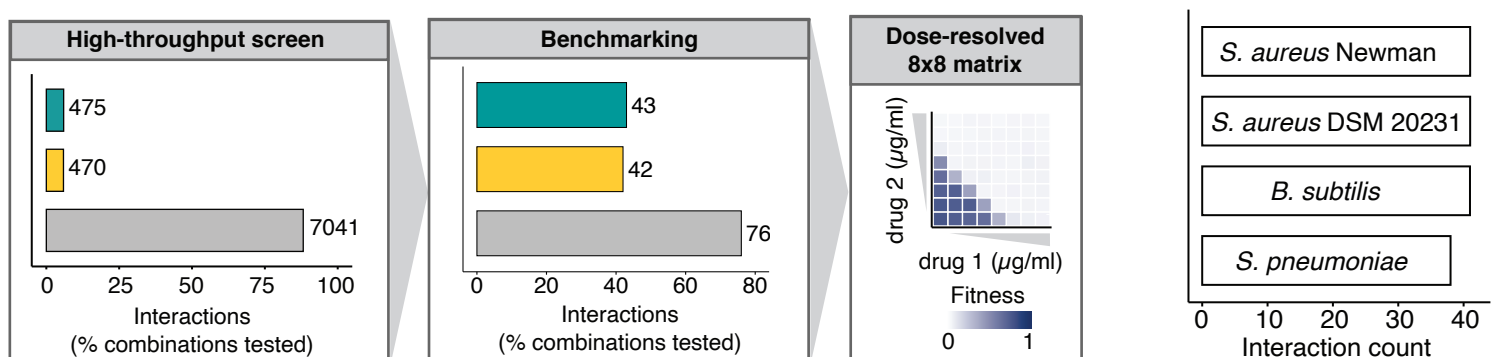
f



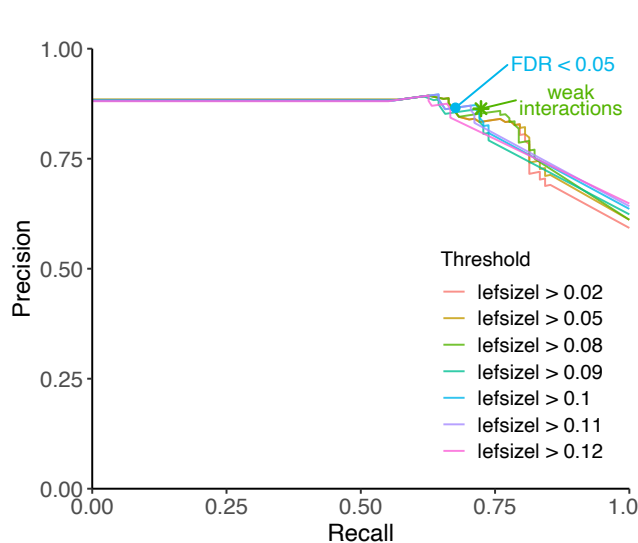
g



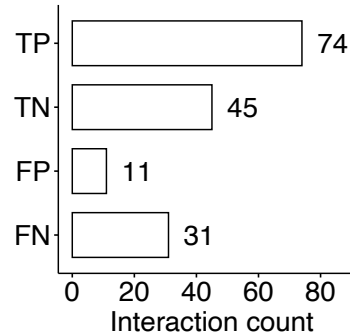
a



c



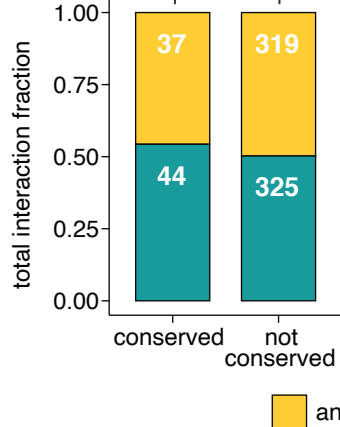
d



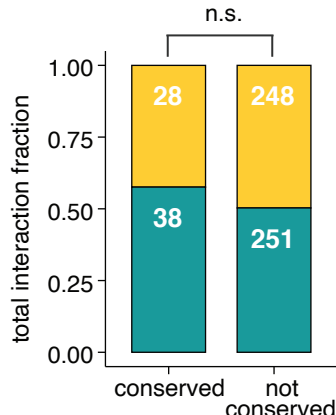
a

Interaction conservation in Gram-positive bacteria

including non-antibiotic drugs

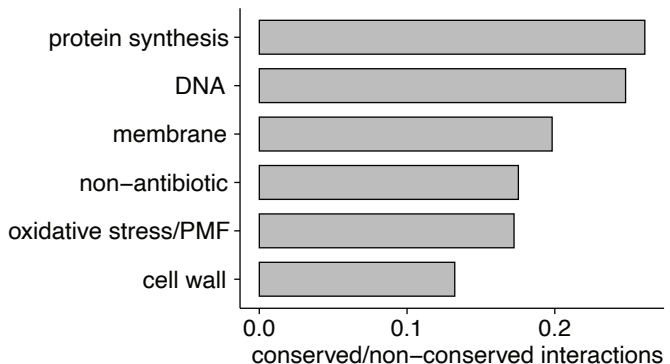


excluding non-antibiotic drugs



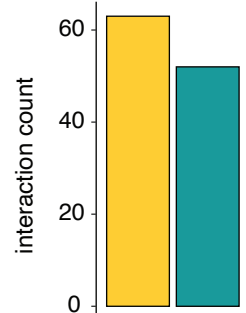
b

Interaction conservation ratio of drug classes in Gram-positive bacteria



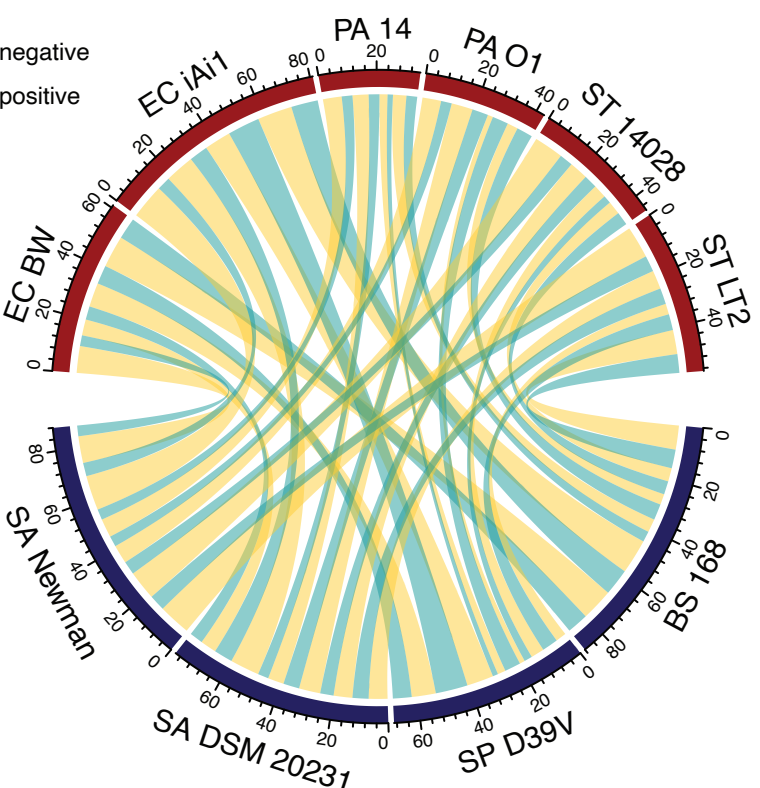
c

Conserved interaction across Gram-positive/-negative species



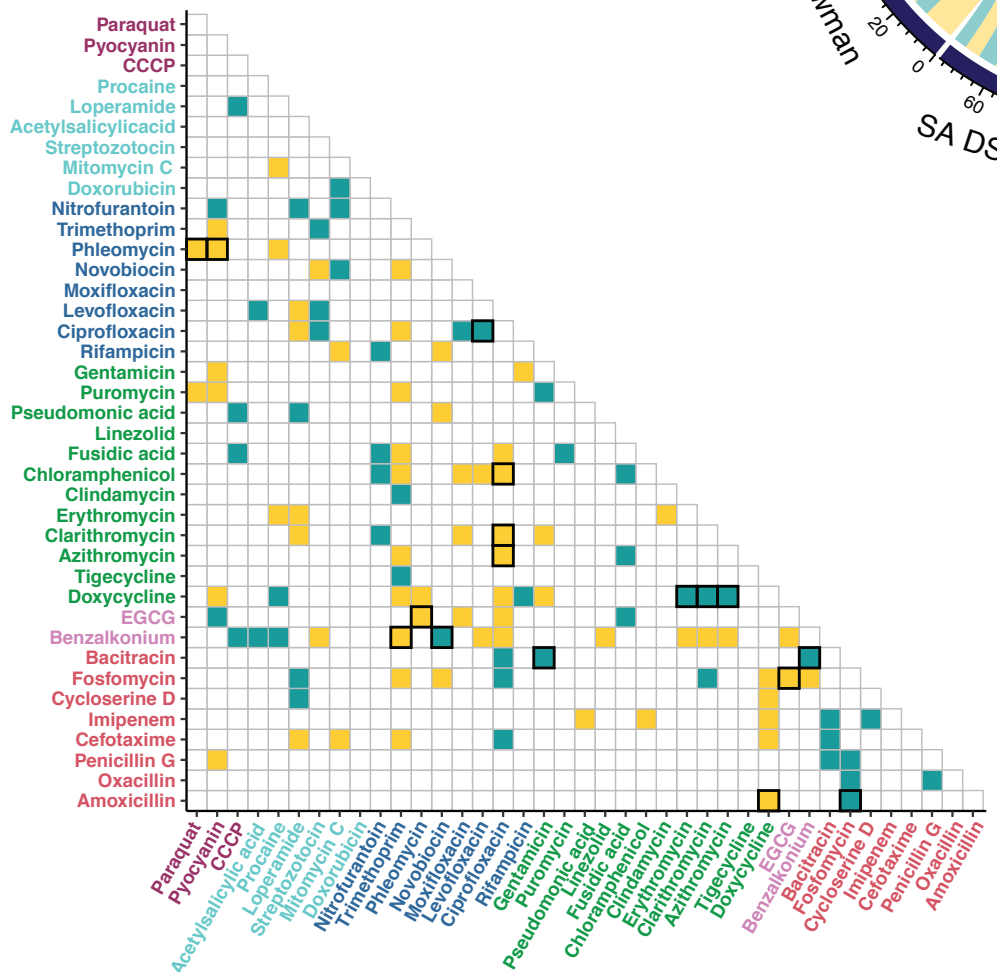
d

Gram-negative
Gram-positive



e

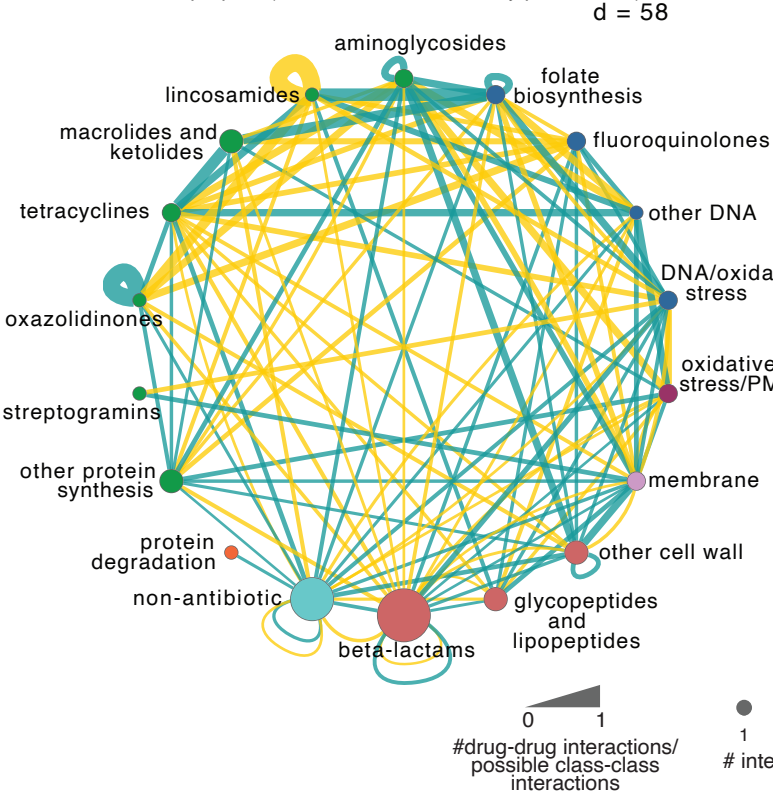
Conserved interaction across Gram-positive/-negative species



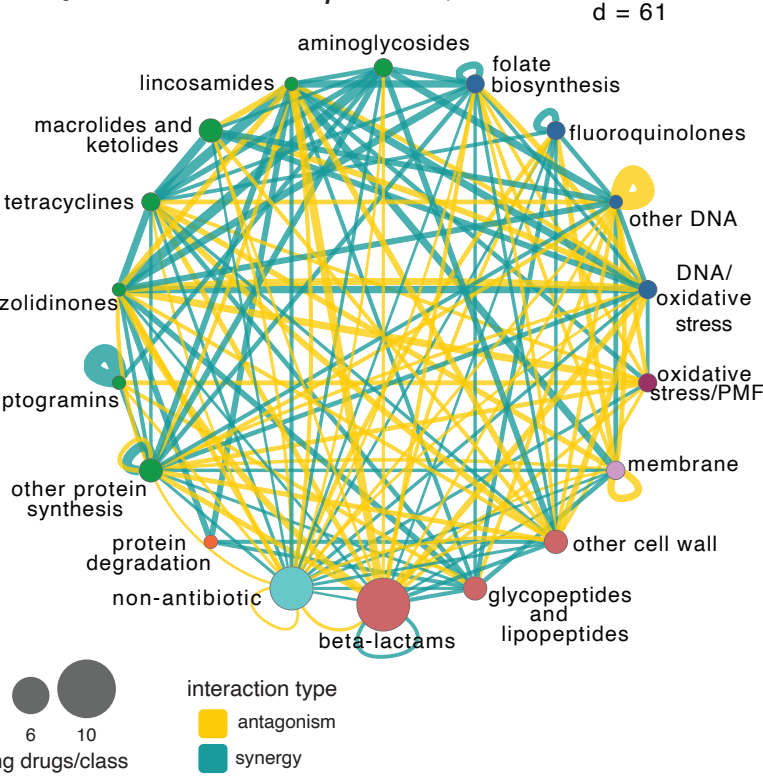
antagonism
synergy
found in >1 Gram-positive species

- oxidative stress/PMF
- non-antibiotic
- DNA
- protein synthesis
- membrane
- cell wall

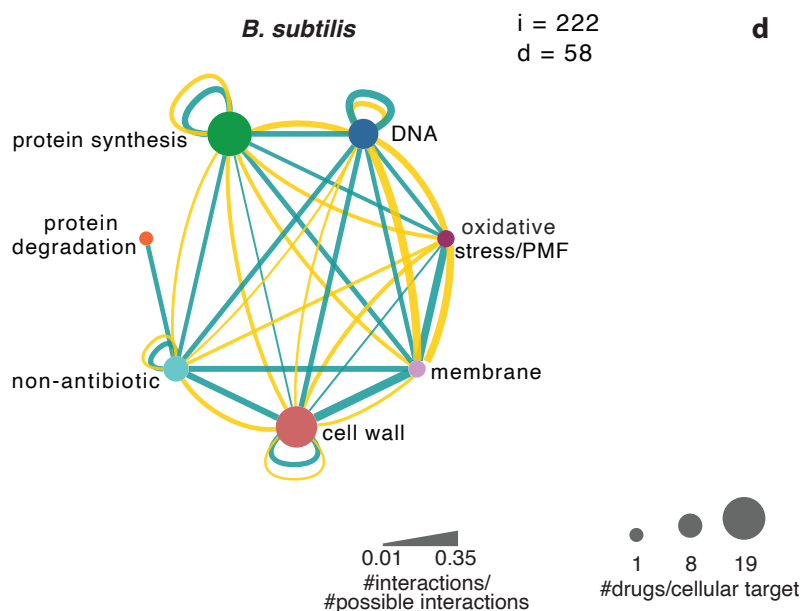
a



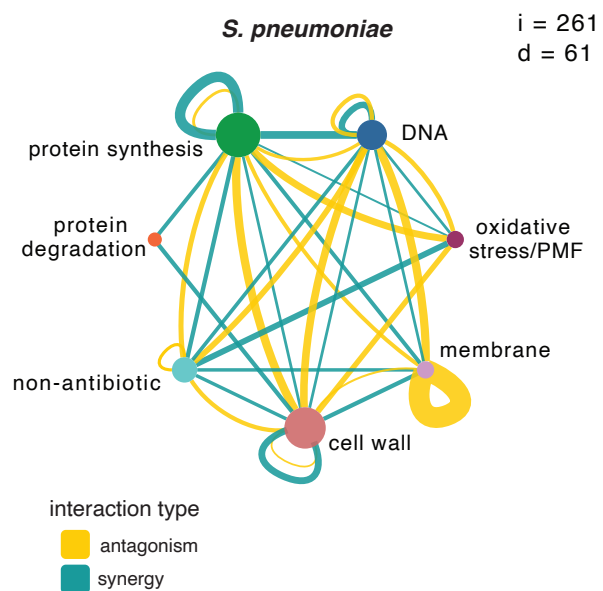
b



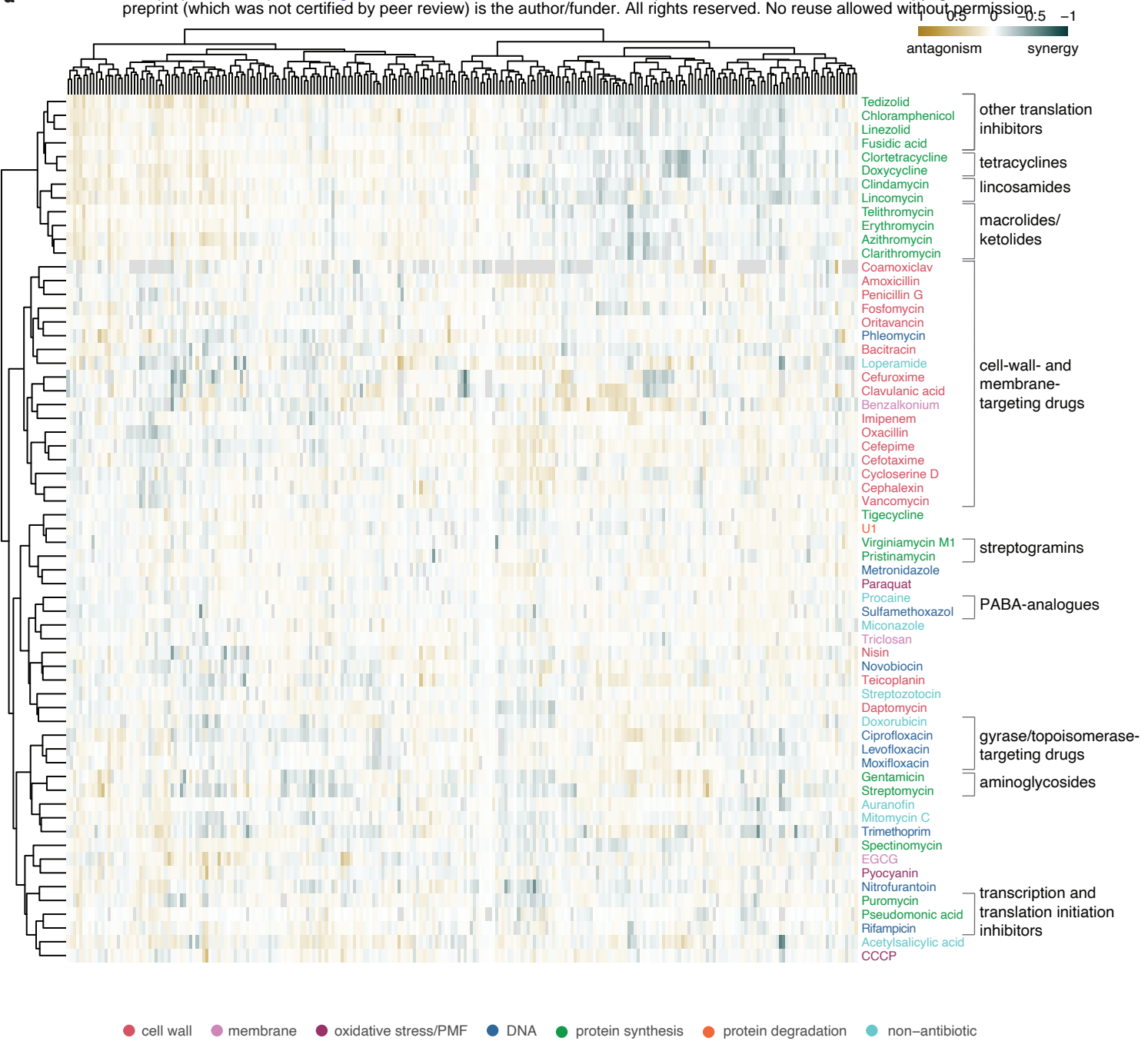
c



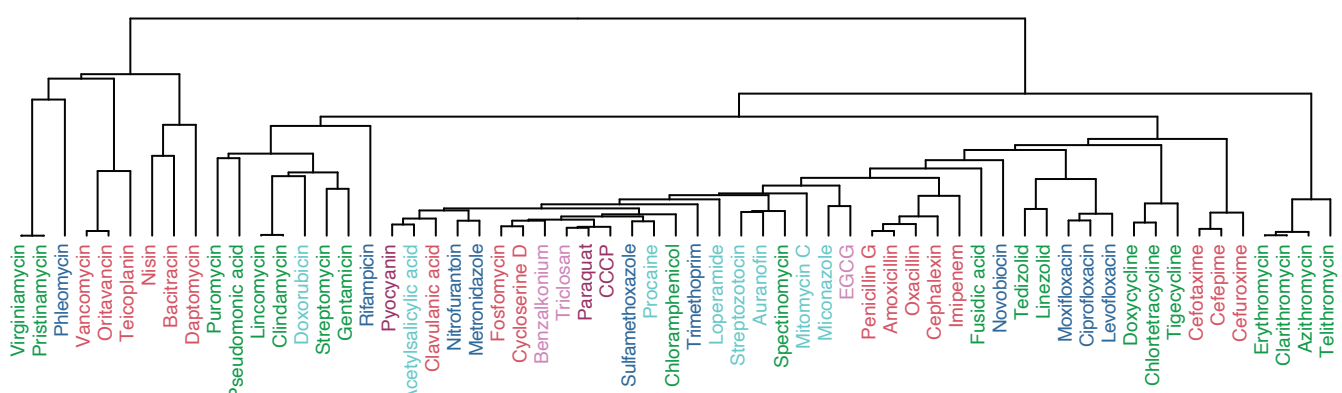
d



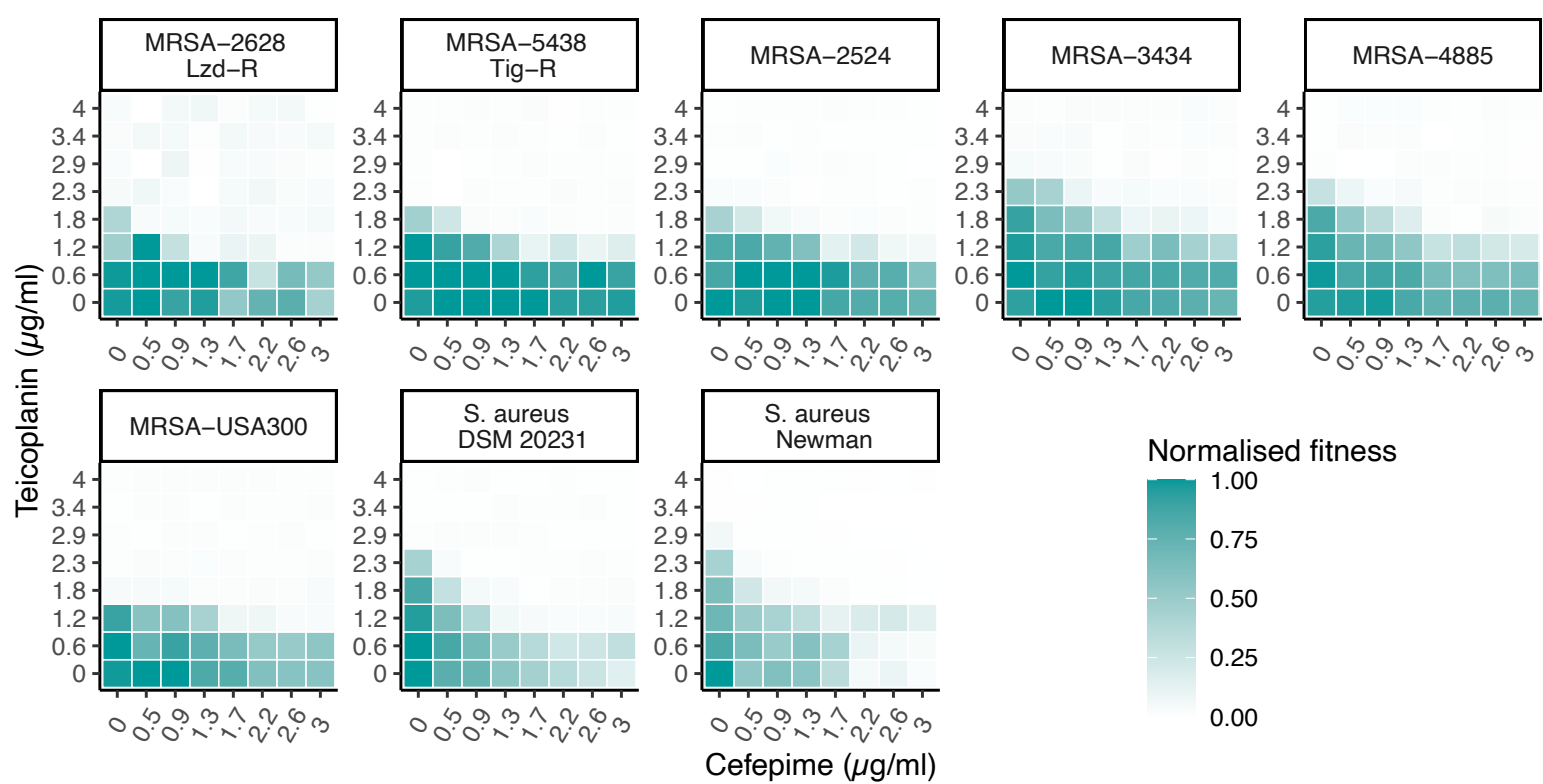
a



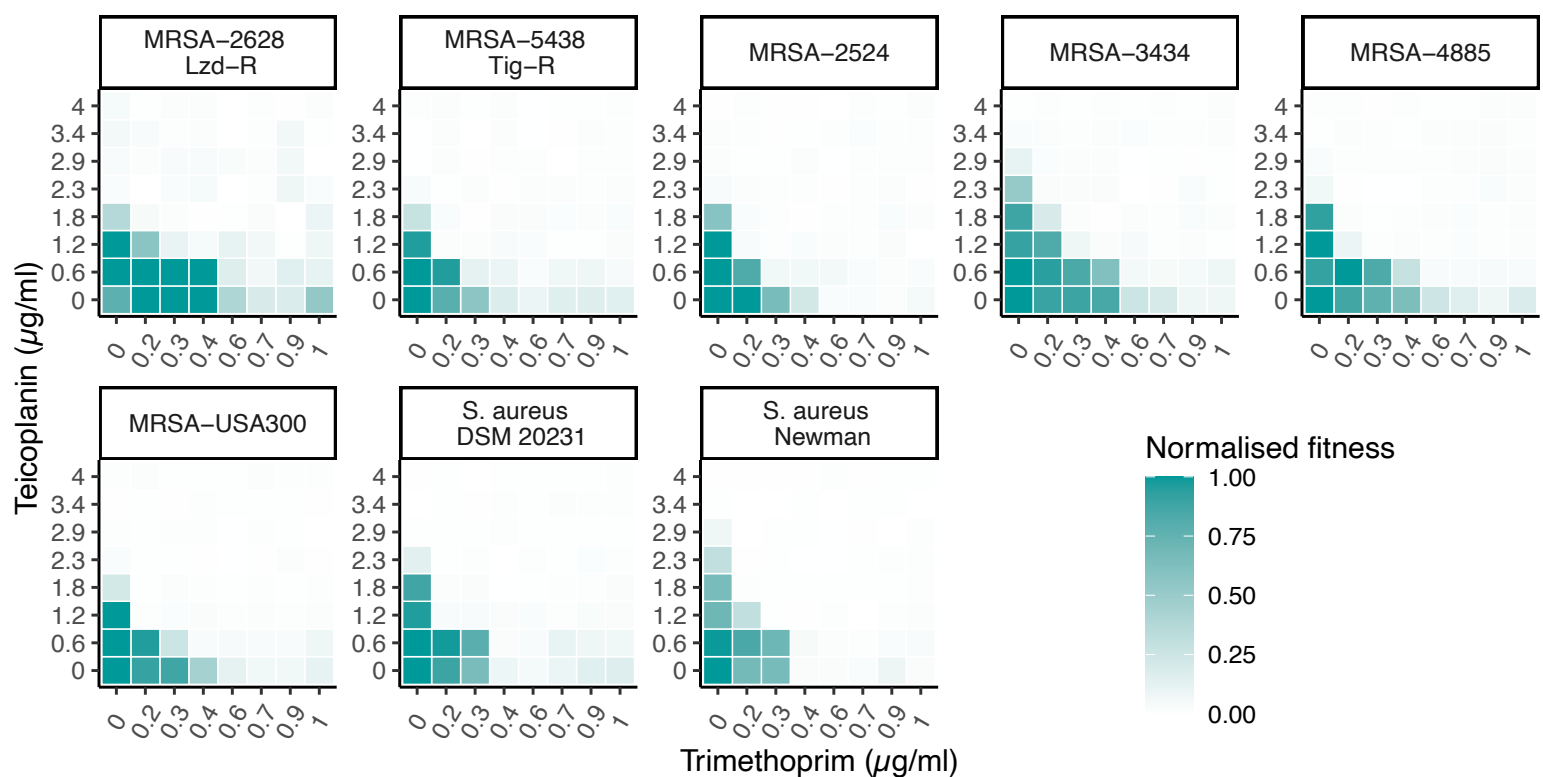
b

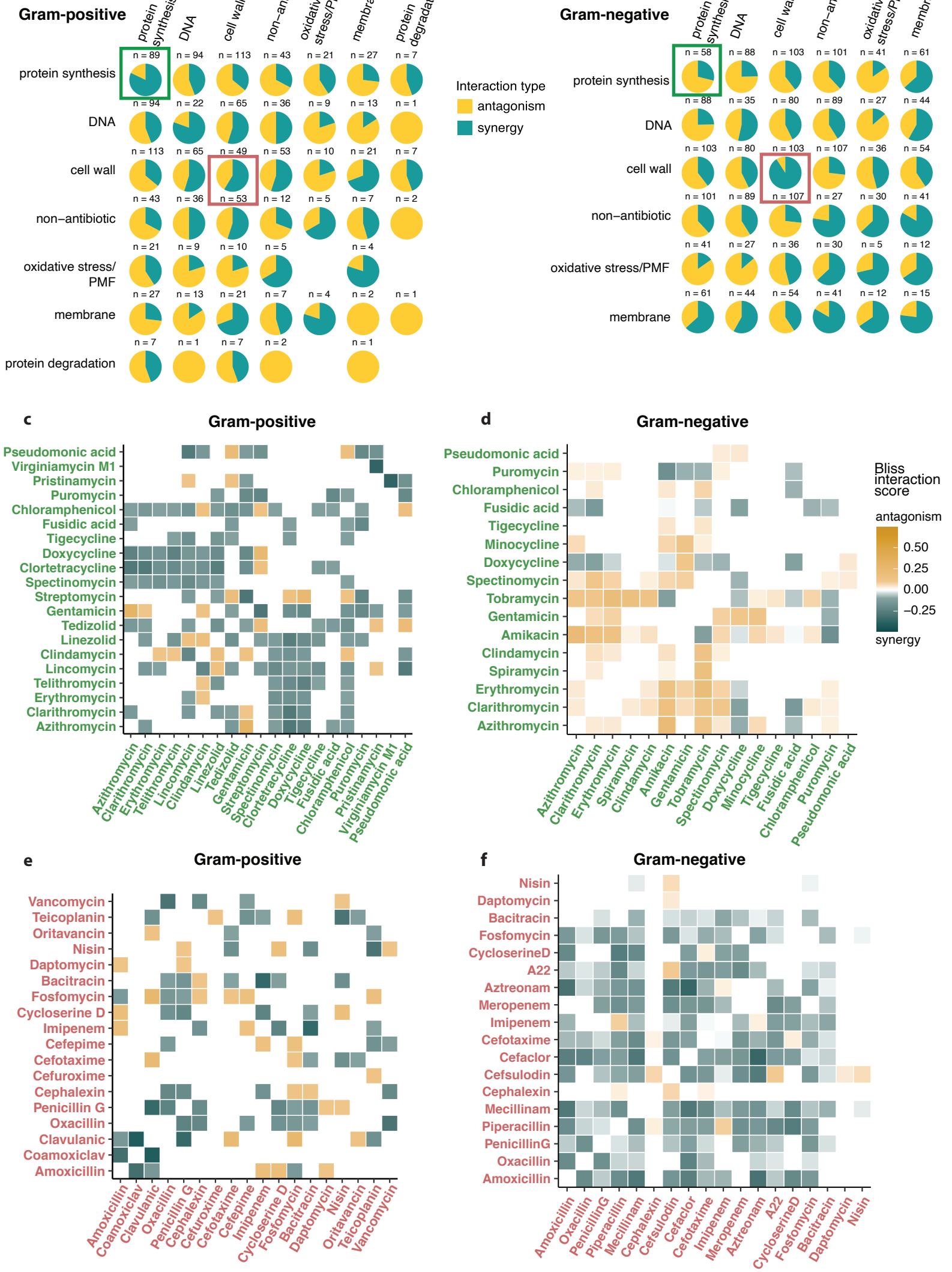


a

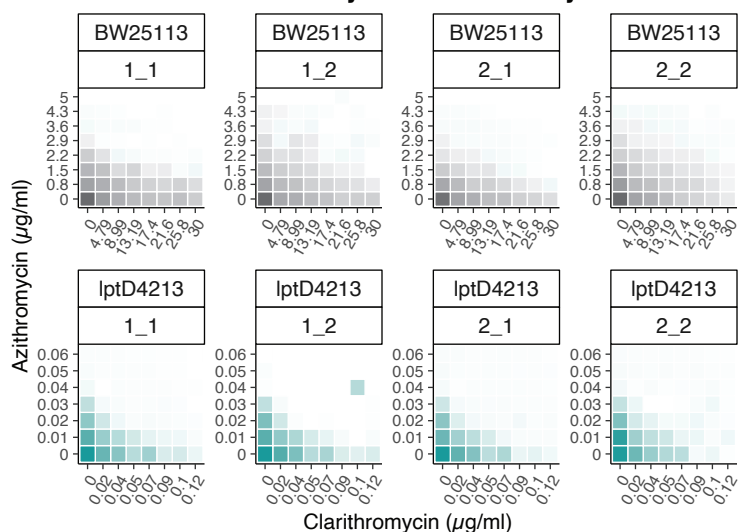


b

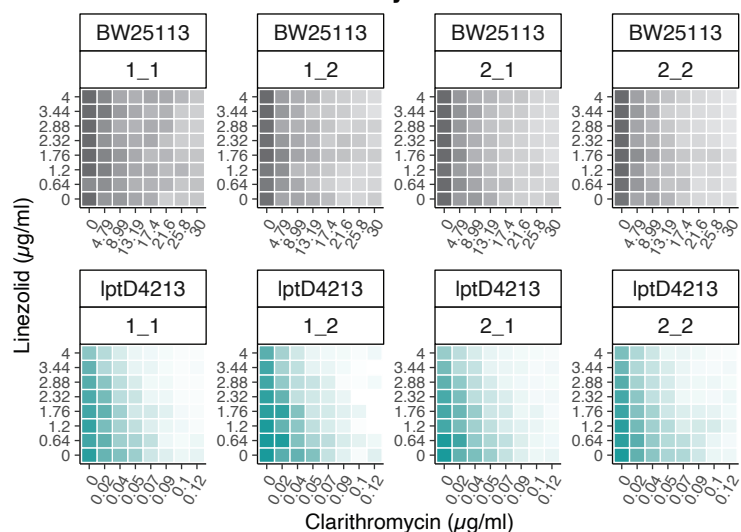




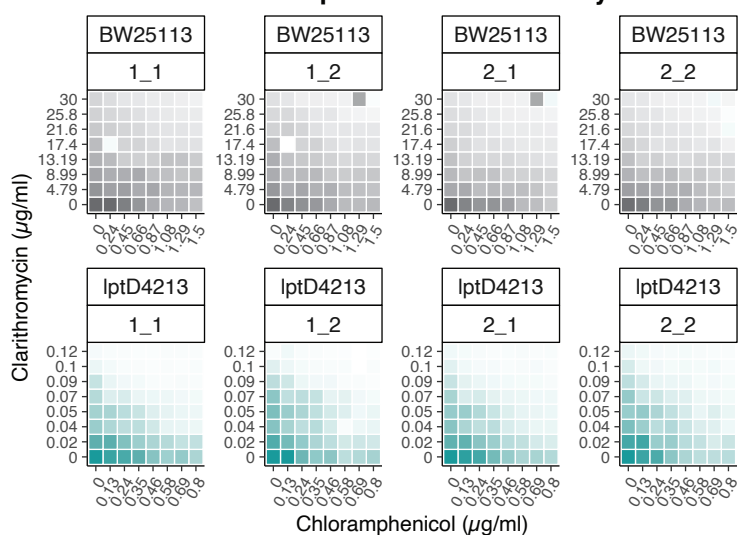
Azithromycin + Clarithromycin



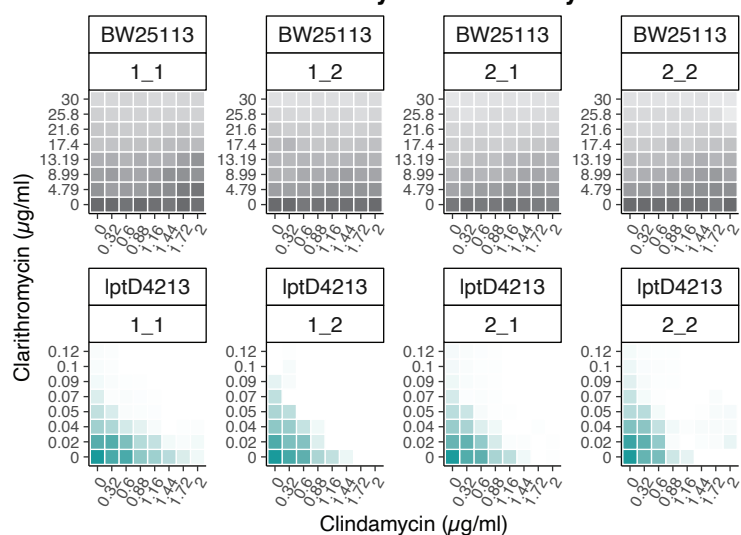
Clarithromycin + Linezolid



Chloramphenicol + Clarithromycin



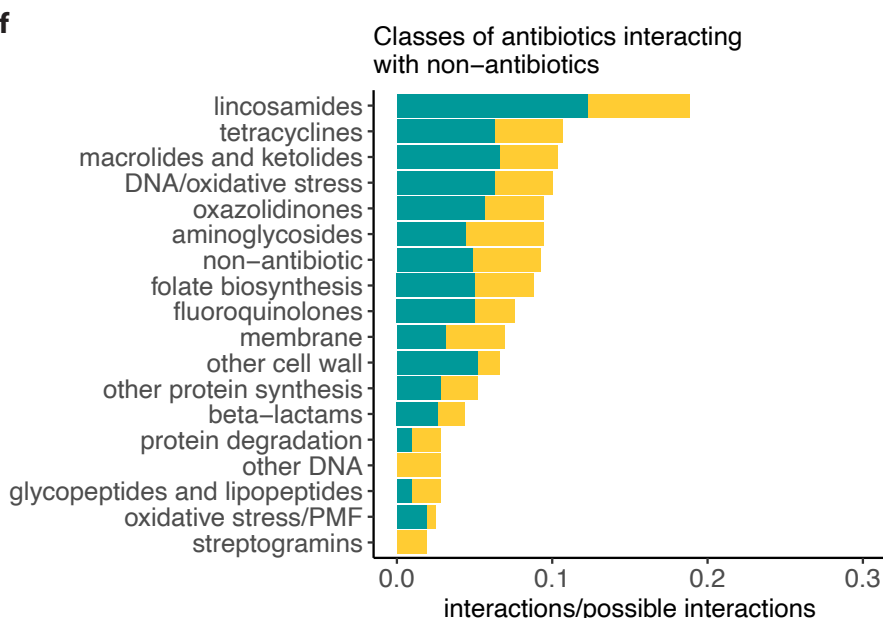
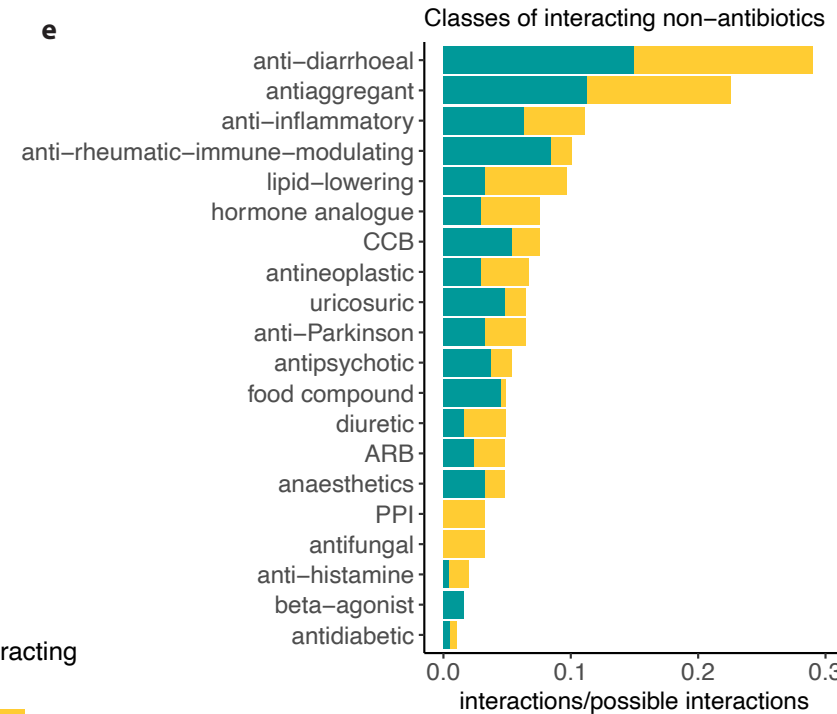
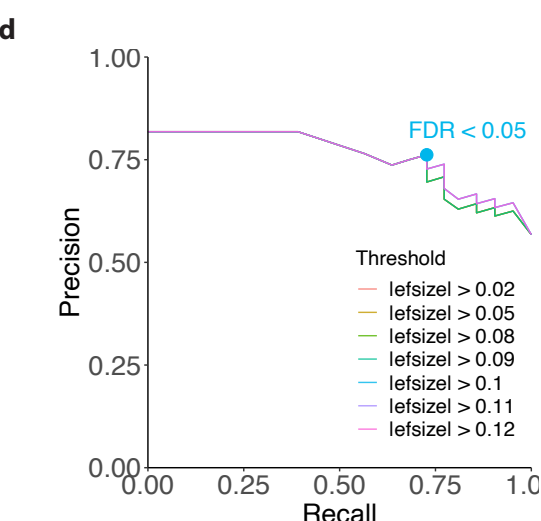
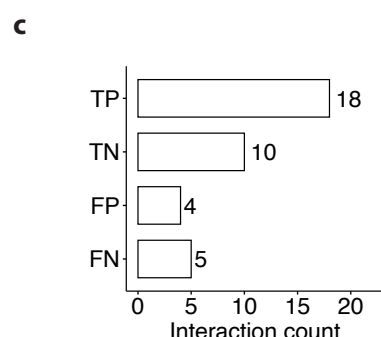
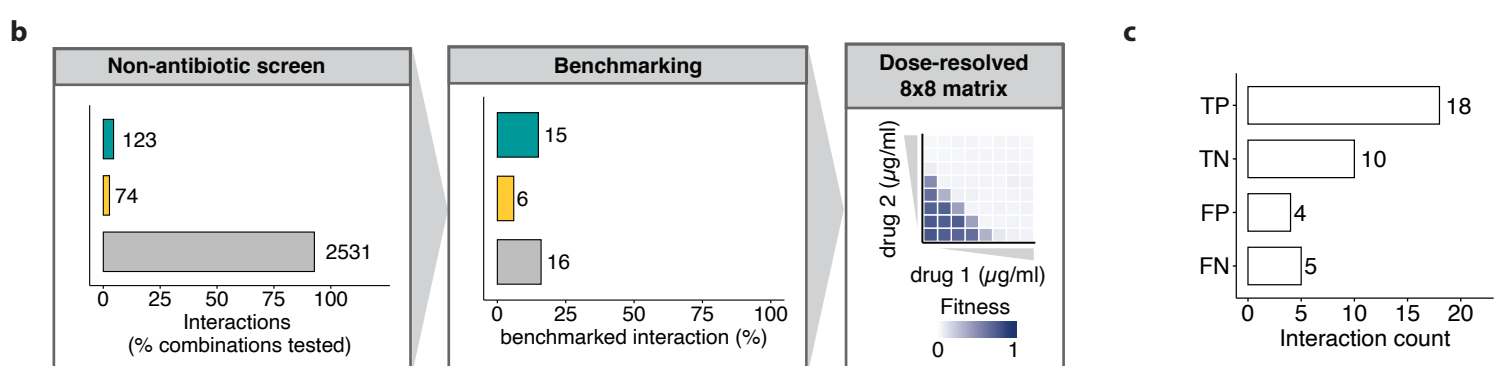
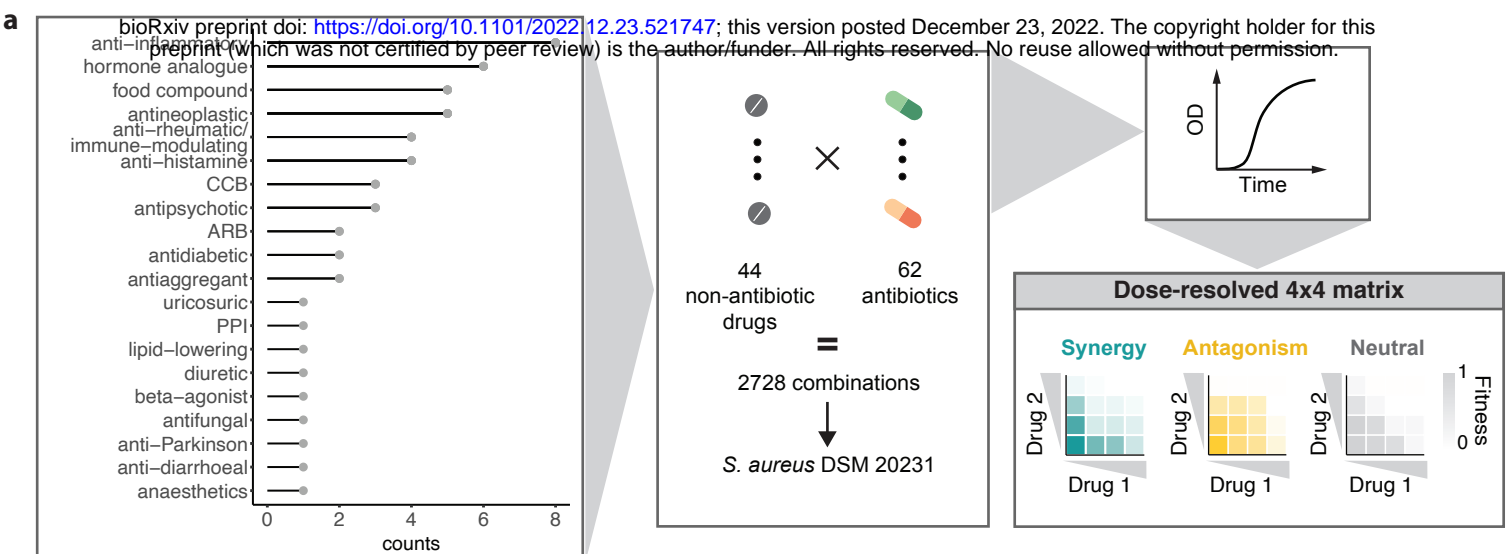
Clarithromycin + Clindamycin



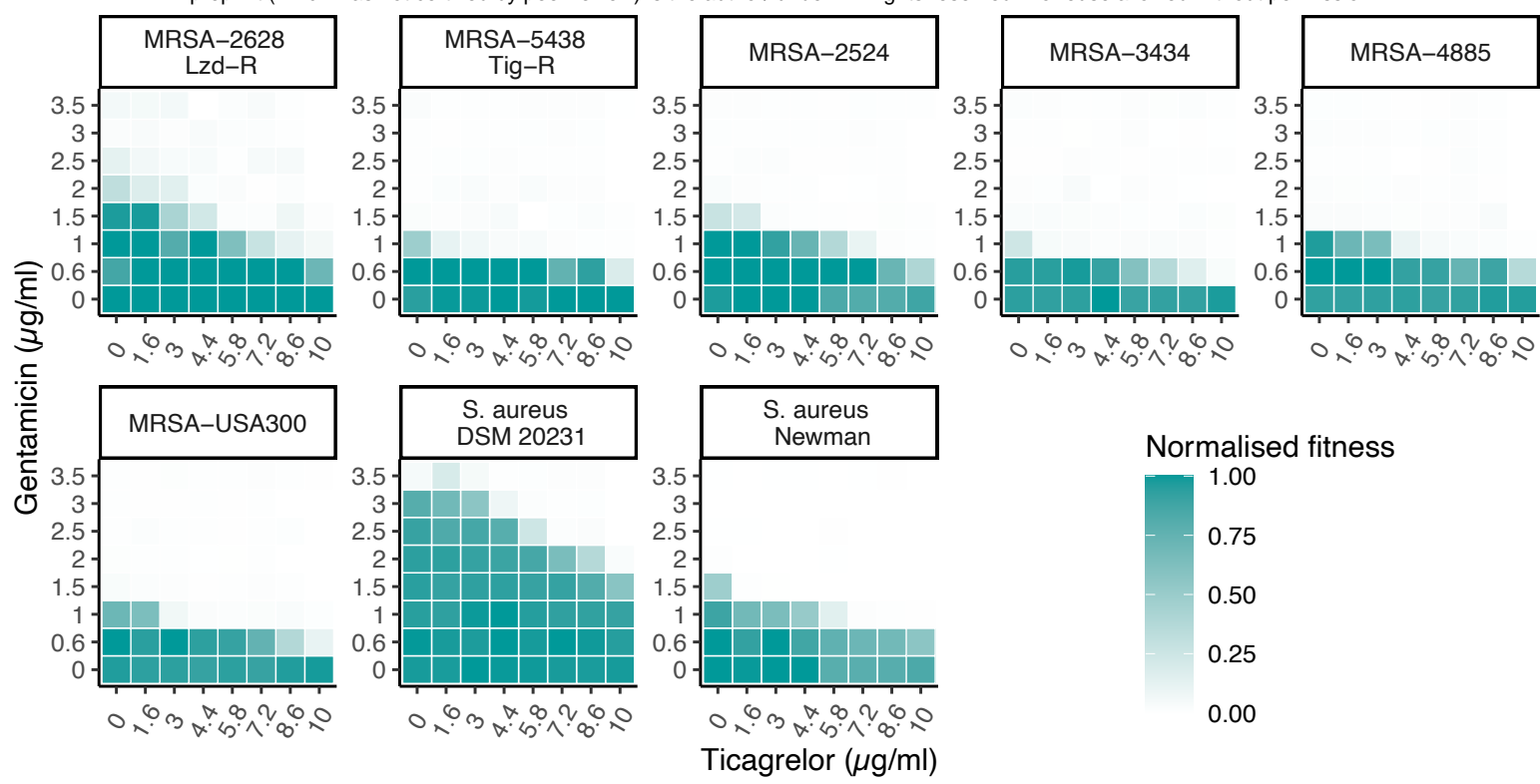
Normalised fitness

1 0.75 0.5 0.25 0

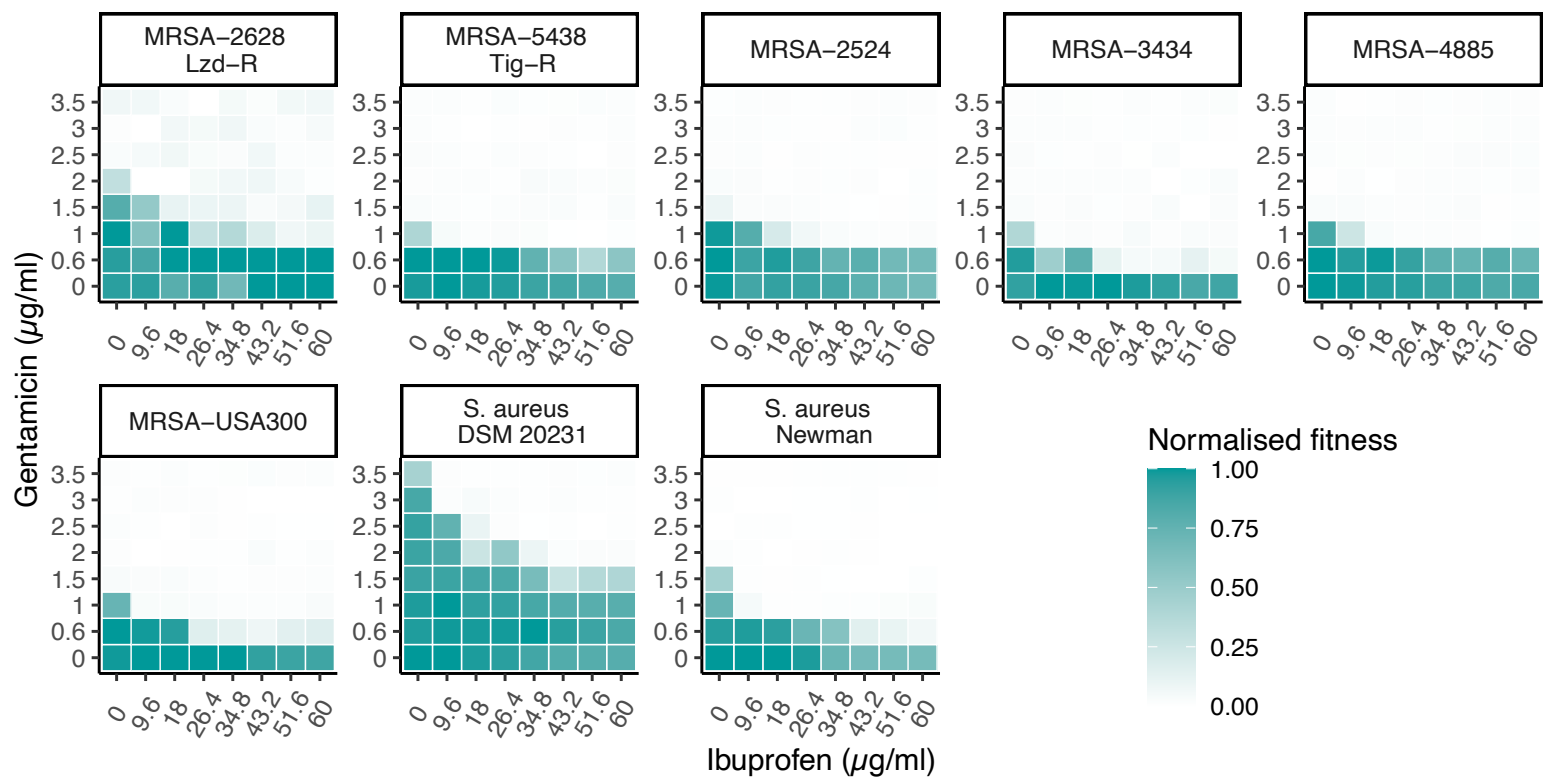
1 0.75 0.5 0.25 0



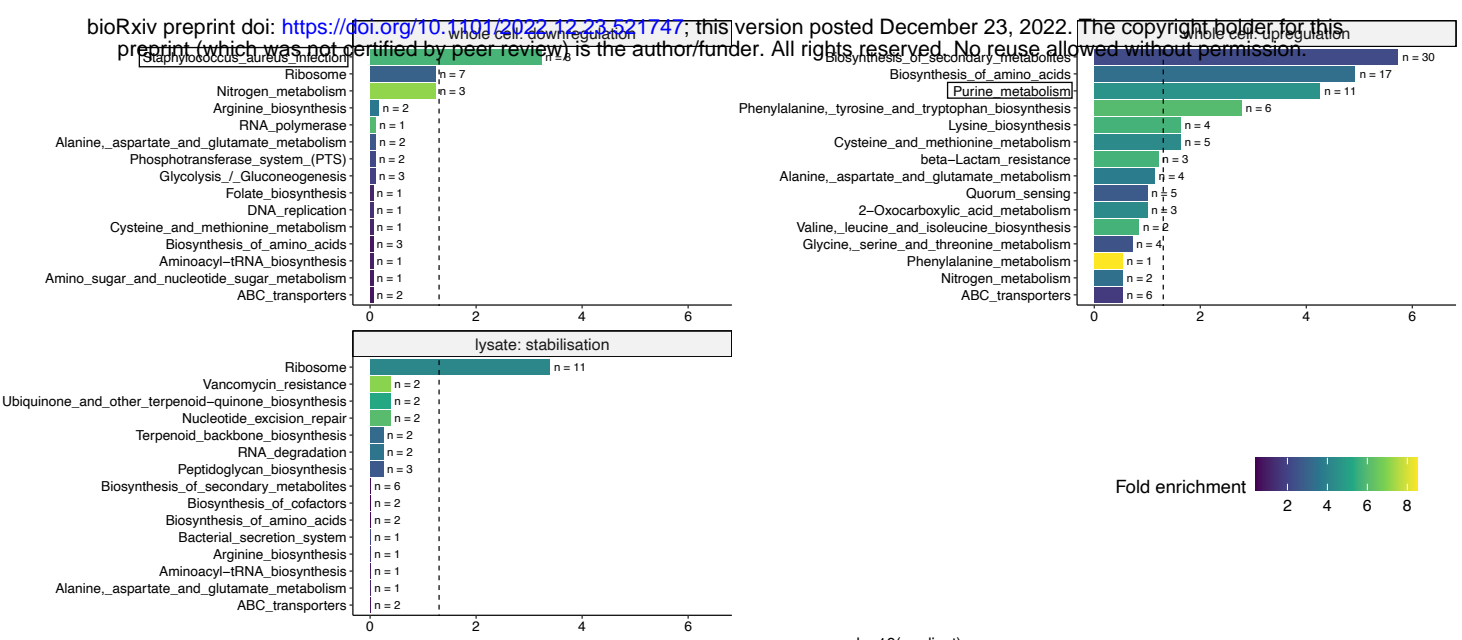
a



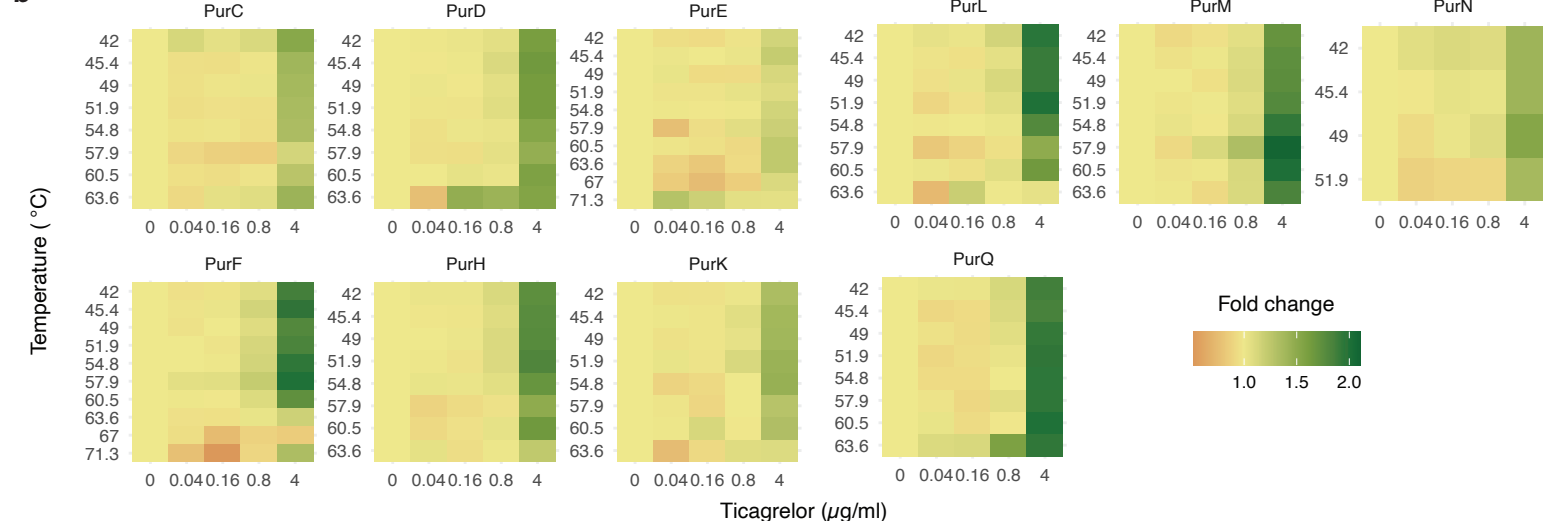
b



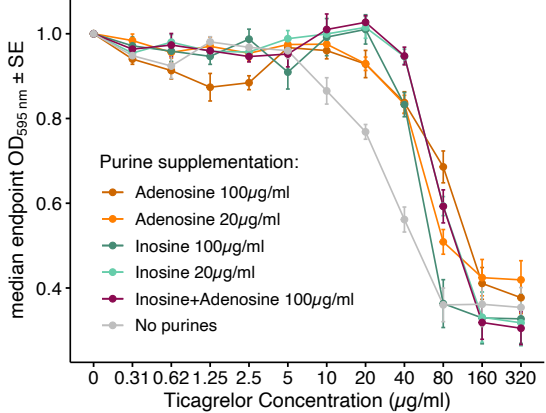
a



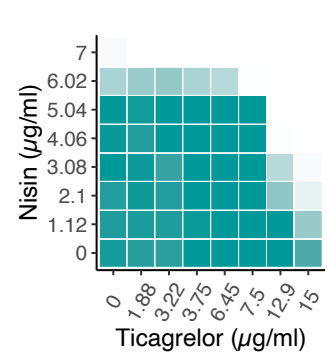
b



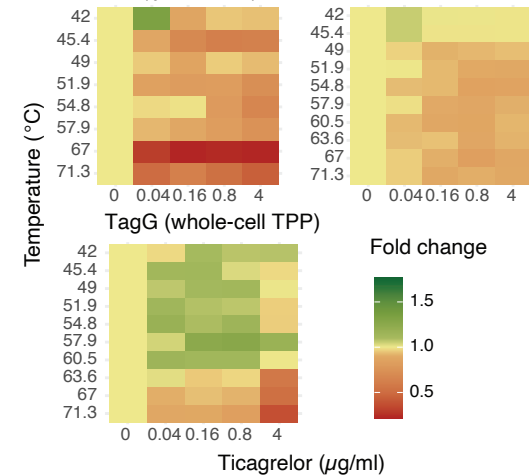
c



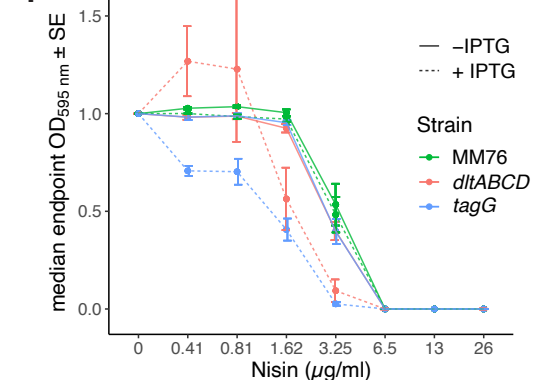
d



e



f



g

